Table 1 Subject profile

	Normal controls	MSA		
		Total	MSA-P	MSA-C
n	8	8	4	4
Gender (F/M)	4/4	4/4	1/3	3/1
Age (years)	64.3 ± 5.90	57.4 ± 10.1	60.5 ± 11.1	54.3 ± 9.50
Duration (years)		1.50 ± 0.54	1.75 ± 0.50	1.25 ± 0.50
UMSARS score		36.1 ± 8.87	41.5 ± 9.39	30.8 ± 4.27

Data are mean ± SD.
MSA-P = MSA with predominant parkinsonism; MSA-C = MSA with predominant cerebellar ataxia; UMSARS = unified MSA rating scale.

subgroup and the MSA with predominant cerebellar ataxia subgroup. The normal control group comprised volunteers without impairment of cognitive and motor functions who had no cerebrovascular lesions on magnetic resonance imaging. The study protocol was approved by the Ethical Committee of Tohoku University Graduate School of Medicine, and a written informed consent was obtained from each subject after being given a complete description of the study.

Radiosynthesis of [¹¹C]-BF-227

BF-227 and its N-desmethylated derivative (a precursor of [¹¹C]-BF-227) were custom-synthesized by Tanabe R&D Service Co. (Tokyo) (Kudo et al., 2007). [¹¹C]-BF-227 was synthesized from the precursor by N-methylation in dimethyl sulphoxide using [¹¹C]-methyl triflate (Jewett, 1992; Iwata et al., 2001). After quenching the reaction with 5% acetic acid in ethanol, [¹¹C]-BF-227 was separated from the crude mixture by semi-preparative reversed-phase high-performance liquid chromatography and then isolated from the collected fraction by solid-phase extraction. The purified [¹¹C]-BF-227 was solubilized in isotonic saline containing 1% polysobate-80 and 5% ascorbic acid. The saline solution was filter sterilized with a 0.22 mm Millipore® filter for clinical use. The radiochemical yields were >50% based on [¹¹C]-methyl triflate, and the specific radioactivities were 119–138 GBq/mmol at the end of synthesis. The radiochemical purities were >95%.

PET procedure

The [¹¹C]-BF-227 PET study was performed using a SET-2400W PET scanner (Shimadzu Inc., Japan) under resting condition with eyes closed in a dark room. Following a 68Ge/Ga transmission scan of 300–400 s duration, an emission scan was started soon after intravenous injection of 3.7–8.3 mCi of [¹¹C]-BF-227. A dynamic series of PET scans were acquired over 60 min with 23 frames. Emission data were corrected for attenuation, dead time and radioactive decay. Standardized uptake value images were obtained by normalizing tissue concentration by the injected dose and body mass. Arterial blood samples (1.5 ml) from the radial or brachial artery were collected from each subject at 10 s intervals for the first 2 min, and subsequently at intervals increasing progressively from 1 to 10 min until 60 min after the injection of [¹¹C]-BF-227 except for one subject, from whom arterialized venous blood samples (1.5 ml) from a hand vein heated in a far-infrared mat were collected at the same time intervals. The plasma obtained by centrifugation at 3000g for 3 min was weighed and the radioactivity was measured with a well-type scintillation counter. Additional arterial blood samples were obtained at four time points during the study (5, 15, 30 and 60 min) for the determination of radiolabelled metabolites in plasma using high-performance liquid

chromatography. These data yielded values of the unchanged fraction of parent radiotracer throughout the time frame of the study. A multi-exponential equation was used to describe this curve and to estimate the parent fraction at each measured plasma curve time point.

PET image analysis

To measure α-synuclein deposition densities in the brain, the distribution volume, the ratio of [¹¹C]-BF-227 concentration in tissue to that in plasma at equilibrium, was calculated by Logan's graphical analysis (Logan, 2000), since BF-227 reversibly binds to α-synuclein depositions (Tashiro et al., 2009). Region of interest analysis was performed to evaluate the regional distribution of [¹¹C]-BF-227. Circular regions of interest were placed on individual axial PET images in the frontal cortex, primary motor cortex, parietal cortex, medial temporal cortex, lateral temporal cortex, occipital cortex, anterior cingulate cortex, posterior cingulate cortex, subcortical white matter, caudate nucleus, putamen, globus pallidus, thalamus, substantia nigra, midbrain tegmentum, pons and cerebellar cortex, referring to the individual magnetic resonance images.

Statistical analysis

Data were expressed as mean ± SD. Differences in distribution volume between normal control and MSA groups were evaluated by one-way analysis of variance followed by Bonferroni's multiple comparison test (GraphPad Prism Software).

Results

Neuropathological staining

In the post-mortem brains with Parkinson's disease, double-labelling immunostaining with BF-227 fluorostaining and anti-phosphorylated α-synuclein antibody demonstrated co-localization of the proteins in Lewy bodies in the substantia nigra (Fig. 1A and B). Strong BF-227 staining was observed in the central core (Fig. 1A). BF-227 was also detected in the cortical Lewy bodies in dementia with Lewy bodies (Fig. 1C and D). In MSA, double-labelling experiments using BF-227 and anti-phosphorylated α-synuclein antibody demonstrated BF-227 fluorescent signal in the most of glial cytoplasmic inclusions in the pontine base (Fig. 1E and F).

PET study

Tissue time activity curves of [¹¹C]-BF-227 in the brain indicated more gradual clearance from the brain in patients with MSA compared with normal subjects following initial rapid uptake of radioactivity (Fig. 2A). Relatively high concentrations of [¹¹C]-BF-227 radioactivity were observed in the subcortical white matter and lenticular nucleus in MSA, in which relatively intense α-synuclein deposits were found in the post-mortem brain (Fig. 2B). [¹¹C]-BF-227 exhibited linear regression curves on Logan plot analysis in all brain regions examined. Since the slopes of the regression lines represent the distribution volume of the tracer, these findings indicated a higher distribution volume of [¹¹C]-BF-227 in MSA than in normal controls (Fig. 2C). The regional distribution volume values were high in the subcortical white matter (uncorrected $P < 0.001$), putamen and posterior cingulate cortex
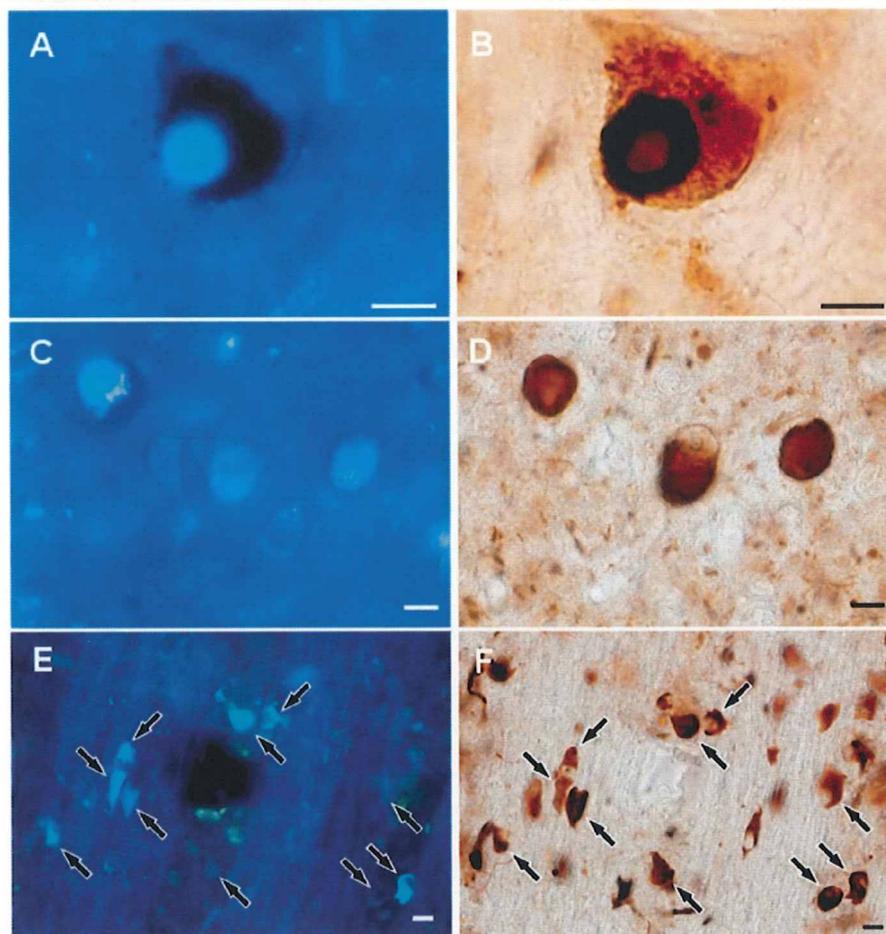
Figure 1 Neuropathological findings of BF-227 fluorostaining and anti-phosphorylated α-synuclein antibody immunostaining. BF-227 fluorostaining (**A** and **C**) and anti-phosphorylated α-synuclein antibody immunostaining (**B** and **D**) showed colocalization of these proteins in brainstem-type Lewy bodies in the substantia nigra of patients with Parkinson's disease (**A** and **B**) and in cortical Lewy bodies in the temporal lobe of patients dementia with Lewy bodies (**C** and **D**). Similarly, BF-227 fluorostaining (**E**) and anti-phosphorylated α-synuclein antibody immunostaining (**F**) were codetected in glial cytoplasmic inclusions in the pontine base of a patient with MSA. BF-227 histofluorescence was observed in the most of glial cytoplasmic inclusions (arrows). Bars = 10 µm.

(uncorrected $P < 0.005$), globus pallidus, primary motor cortex and anterior cingulate cortex (uncorrected $P < 0.01$) and substantia nigra (uncorrected $P < 0.05$) in patients with MSA compared to the normal controls (Table 2 and Fig. 2D). It is noteworthy that the distribution volume of [^{11}C]-BF-227 was significantly high in the subcortical white matter even if Bonferroni's multiple comparison test was applied. On the other hand, no obvious differences were found in either the distribution or degree of binding between the MSA with predominant parkinsonism and MSA with predominant cerebellar ataxia subgroups.

Discussion

The BF-227 stained α-synuclein-containing Lewy bodies (Fig. 1A–D) and glial cytoplasmic inclusions (Fig. 1E and F) in formalin-fixed tissue sections as well as β-amyloid-containing

senile plaques in paraffin-embedded tissue sections (Kudo *et al.*, 2007). These results were consistent with the previous findings showing BF-227 binding to synthetic α-synuclein fibrils with high affinity (K_d 9.63 nM) (Fodero-Tavoletti *et al.*, 2009), and to Lewy bodies in paraffin-embedded tissue sections (Fodero-Tavoletti *et al.*, 2009).

The anti-phosphorylated α-synuclein antibody immunostained the halo region more intensively compared with the central core in Lewy bodies in the substantia nigra of Parkinson's disease, while the BF-227 staining was intensely observed in the core of Lewy bodies (Fig. 1A and B). Because intense thioflavin S staining was also reported in the core of nigral Lewy bodies (Duda *et al.*, 2000), the core is thought to be rich in β-sheet structures. Similar to thioflavin S, the BF-227 staining is considered to recognize amyloid-like β-pleated sheets, and it was suggested to be the reason for the more intense BF-227 staining in the core of Lewy bodies. In addition, the high density of the core structure
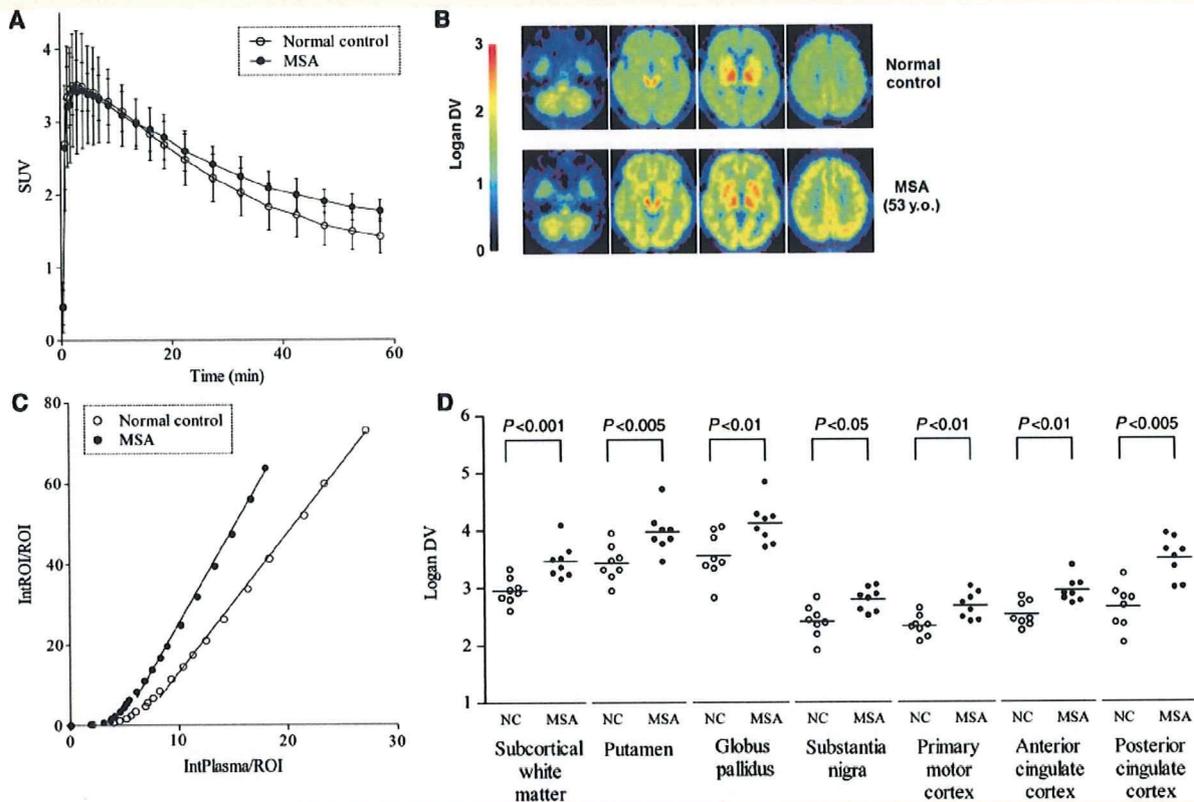
Figure 2 [¹¹C]-BF-227 PET findings in MSA. Time activity curves showed initial rapid uptake of radioactivity followed by gradual clearance in the putamen of both normal subjects and MSA cases. Data are mean ± SD of eight normal subjects and eight patients with MSA (**A**). In a representative patient with MSA with predominant cerebellar ataxia, the regional distribution volumes were mapped to the subcortical white matter and lentiform nucleus compared to normal control (**B**). Typical Logan plots for the putamen were presented in a representative patient with MSA with predominant cerebellar ataxia and a normal control. The slopes of the linear regression curves on Logan plot analysis represent the distribution volume of the tracer in the putamen (**C**). There were differences in the mean regional distribution volume values between patients with MSA and normal control in the subcortical white matter (uncorrected $P < 0.001$), putamen and posterior cingulate cortex (uncorrected $P < 0.005$), globus pallidus, primary motor cortex and anterior cingulate cortex (uncorrected $P < 0.01$) and substantia nigra (uncorrected $P < 0.05$). Data of individual subjects (symbols) and mean values (horizontal lines) (**D**). SUV = standardized uptake value; DV = distribution volume; ROI = region of interest.

may often prevent the penetration of antibodies into this region (Galloway *et al.*, 1992), since electron microscopic studies revealed that vesicular structures were tightly packed in the core of Lewy bodies (Takahashi and Wakabayashi, 2005). On the other hand, not all glial cytoplasmic inclusions stained by anti-phosphorylated α-synuclein antibody were always positive for BF-227 staining (Fig. 1E and F). In the process of oligodendroglial pathology, it was believed that α-synuclein deposits as amorphous state and then forms fibrillar structures (Gai *et al.*, 2003; Stefanova *et al.*, 2005). In fact, part of glial cytoplasmic inclusions were reported to be α-synuclein-negative (Sakamoto *et al.*, 2005) and therefore, it seems reasonable that some of glial cytoplasmic inclusions were not composed of β-sheet fibrils and were negative for BF-227 staining.

The regional distribution volume of [¹¹C]-BF-227 was the highest in the subcortical white matter, followed by the putamen, posterior cingulate cortex, anterior cingulate cortex, globus

pallidus, primary motor cortex and substantia nigra, in which glial cytoplasmic inclusions were densely distributed (Papp and Lantos, 1994; Inoue *et al.*, 1997; Wakabayashi and Takahashi, 2006) and large increases of α-synuclein content were found (Tong *et al.*, 2010) in the post-mortem brains. Thus, it was suggested that the distributions of [¹¹C]-BF-227 could properly reflect those of the α-synuclein deposits *in vivo*. On the other hand, the regional distribution volume in other affected brain regions, such as the cerebellum and pons (Ozawa *et al.*, 2004; Wakabayashi and Takahashi, 2006), did not show higher values relative to the normal control group. The glial cytoplasmic inclusions in cerebellum were reported to decrease along with the disease progression and concomitant neuronal loss (Inoue *et al.*, 1997). Therefore, it is plausible that the accumulation levels of glial cytoplasmic inclusions are changing and do not always increase with the disease progression (Mochizuki *et al.*, 1992; Inoue *et al.*, 1997). Moreover, due to the remarkable cerebellar and pontine atrophy,

Table 2 Distribution volume of [^{11}C]BF-227

	Normal controls	MSA
Frontal cortex	2.28 ± 0.18	2.46 ± 0.22
Primary motor cortex	2.40 ± 0.28	2.79 ± 0.20¶
Parietal cortex	2.48 ± 0.26	2.63 ± 0.24
Medial temporal cortex	2.44 ± 0.21	2.82 ± 0.31
Lateral temporal cortex	2.42 ± 0.19	2.63 ± 0.23
Occipital cortex	2.43 ± 0.20	2.72 ± 0.27
Anterior cingulate cortex	2.32 ± 0.18	2.67 ± 0.23¶
Posterior cingulate cortex	2.52 ± 0.22	2.94 ± 0.22†
Subcortical white matter	2.65 ± 0.38	3.49 ± 0.36‡
Caudate nucleus	2.70 ± 0.21	3.05 ± 0.34
Putamen	2.95 ± 0.23	3.47 ± 0.30†
Globus pallidus	3.43 ± 0.31	3.97 ± 0.36¶
Thalamus	3.50 ± 0.28	4.03 ± 0.31
Substantia nigra	3.55 ± 0.41	4.12 ± 0.36*
Midbrain tegmentum	3.53 ± 0.54	3.45 ± 0.47
Pons	3.63 ± 0.54	3.88 ± 0.42
Cerebellar cortex	2.32 ± 0.22	2.16 ± 0.29

Data are mean ± SD.
*Uncorrected $P < 0.05$.
¶Uncorrected $P < 0.01$.
†Uncorrected $P < 0.005$.
‡Uncorrected $P < 0.001$.

the distribution volume in these regions might be underestimated. Correction for partial volume loss is therefore needed to improve the accuracy of quantification in the cerebellum and brainstem of MSA. BF-227 fluorescent signal was detected in β-amyloid plaques as well as glial cytoplasmic inclusions and Lewy bodies (Fig. 1A–F) in neuropathological staining (Kudo *et al.*, 2007). However, the differences in the distribution of [^{11}C]-BF-227 by PET could discriminate MSA from Alzheimer's disease, which showed high distribution of [^{11}C]-BF-227 in the temporoparietal–occipital region (Kudo *et al.*, 2007). In our preliminary studies, Parkinson's disease and dementia with Lewy bodies also showed quite different patterns of distribution volumes from those of MSA (data not shown). Therefore, MSA could be distinguished from other degenerative diseases such as Alzheimer's disease, Parkinson's disease and dementia with Lewy bodies by the [^{11}C]-BF-227 PET.

The affinity of BF-227 to α-synuclein fibrils (K_d 9.63 nM) was reported to be almost identical to that of PIB (K_d 10.07 nM) (Fodero-Tavoletti *et al.*, 2007, 2009). However, in the post-mortem human brain, the PIB binding was not colocalized with α-synuclein-positive Lewy bodies in two reports (Fodero-Tavoletti *et al.*, 2007; Ye *et al.*, 2008) although one report showed PIB binding to Lewy bodies in the substantia nigra of Parkinson's disease (Maetzler *et al.*, 2008). Therefore, there is controversy as to whether PIB binds to α-synuclein-containing Lewy bodies. Moreover, there have been no reports showing that PIB could detect α-synuclein deposits in α-synucleinopathies by PET (Fodero-Tavoletti *et al.*, 2007; Johansson *et al.*, 2008; Maetzler *et al.*, 2008). The hydroxy group in PIB (Mathis *et al.*, 2003) may prevent it from passing through the cell membranes and thereby detecting α-synuclein depositions in the cytoplasm, however, the BF-227 is more

lipophilic than PIB (Mathis *et al.*, 2003), and may easily pass into the cytoplasm and bind to α-synuclein aggregates. As shown in the present study, BF-227 is a promising tracer to detect glial cytoplasmic inclusions. Further studies are warranted to verify whether Lewy bodies in other α-synucleinopathies as well as glial cytoplasmic inclusions can be detected by [^{11}C]-BF-227 PET.

In conclusion, the BF-227 could bind to α-synuclein-containing glial cytoplasmic inclusions (Fig. 1E and F) in the post-mortem brain, and the [^{11}C]-BF-227 PET demonstrated high signals in the glial cytoplasmic inclusion-rich brain regions including subcortical white matter, putamen, globus pallidus, primary motor cortex and anterior and posterior cingulate cortex (Table 2 and Fig. 2D). These results suggest that [^{11}C]-BF-227 PET is a suitable surrogate maker for monitoring α-synuclein deposits in living brains with MSA and could be a potential tool to monitor the effectiveness of neuroprotective therapy for α-synucleinopathies.

Funding

References

Dejerine J, Thomas A. L'atrophie olivo-ponto-cérébelleuse. Nouvelle Iconographie Salpêtrière 1900; 13: 330–7.

Duda JE, Lee VM, Trojanowski JQ. Neuropathology of synuclein aggregates. J Neurosci Res 2000; 61: 121–7.

Fodero-Tavoletti MT, Mulligan RS, Okamura N, Furumoto S, Rowe CC, Kudo Y, et al. In vitro characterisation of BF227 binding to alpha-synuclein/Lewy bodies. Eur J Pharmacol 2009; 617: 54–8.

Fodero-Tavoletti MT, Smith DP, McLean CA, Adlard PA, Barnham KJ, Foster LE, et al. In vitro characterization of Pittsburgh compound-B binding to Lewy bodies. J Neurosci 2007; 27: 10365–71.

Fujishiro H, Ahn TB, Frigerio R, DelleDonne A, Josephs KA, Parisi JE, et al. Glial cytoplasmic inclusions in neurologically normal elderly: prodromal multiple system atrophy? Acta Neuropathol 2008; 116: 269–75.

Gai WP, Pountney DL, Power JH, Li QX, Culvenor JG, McLean CA, et al. alpha-Synuclein fibrils constitute the central core of oligodendroglial inclusion filaments in multiple system atrophy. Exp Neurol 2003; 181: 68–78.

Galloway PG, Mulvihill P, Perry G. Filaments of Lewy bodies contain insoluble cytoskeletal elements. Am J Pathol 1992; 140: 809–22.

Gilman S, Low PA, Quinn N, Albanese A, Ben-Shlomo Y, Fowler CJ, et al. Consensus statement on the diagnosis of multiple system atrophy. J Neurol Sci 1999; 163: 94–8.

Gilman S, Wenning GK, Low PA, Brooks DJ, Mathias CJ, Trojanowski JQ, et al. Second consensus statement on the diagnosis of multiple system atrophy. Neurology 2008; 71: 670–6.

Hirohata M, Ono K, Morinaga A, Yamada M. Non-steroidal anti-inflammatory drugs have potent anti-fibrillogenic and fibril-destabilizing effects for alpha-synuclein fibrils in vitro. Neuropharmacology 2008; 54: 620–7.

Inoue M, Yagishita S, Ryo M, Hasegawa K, Amano N, Matsushita M. The distribution and dynamic density of oligodendroglial cytoplasmic inclusions (GCIs) in multiple system atrophy: a correlation between the density of GCIs and the degree of involvement of striatonigral and olivopontocerebellar systems. Acta Neuropathol 1997; 93: 585–91.

Iwata R, Pascali C, Bogni A, Miyake Y, Yanai K, Ido T. A simple loop method for the automated preparation of (11C)raclopride from (11C)methyl triflate. Appl Radiat Isot 2001; 55: 17–22.

Jewett DM. A simple synthesis of [11C]methyl triflate. Int J Rad Appl Instrum [A] 1992; 43: 1383–5.

Johansson A, Savitcheva I, Forsberg A, Engler H, Langstrom B, Nordberg A, et al. [(11C)]-PIB imaging in patients with Parkinson's disease: preliminary results. Parkinsonism Relat Disord 2008; 14: 345–7.

Kudo Y, Okamura N, Furumoto S, Tashiro M, Furukawa K, Maruyama M, et al. 2-(2-[2-Dimethylaminothiazol-5-yl]ethenyl)-6-(2-[fluoro]ethoxy)benzoxazole: a novel PET agent for in vivo detection of dense amyloid plaques in Alzheimer's disease patients. J Nucl Med 2007; 48: 553–61.

Logan J. Graphical analysis of PET data applied to reversible and irreversible tracers. Nucl Med Biol 2000; 27: 661–70.

Maetzler W, Reimold M, Liepelt I, Solbach C, Leyhe T, Schweitzer K, et al. [11C]PIB binding in Parkinson's disease dementia. Neuroimage 2008; 39: 1027–33.

Marti MJ, Tolosa E, Campdelacreu J. Clinical overview of the synucleinopathies. Mov Disord 2003; 18(Suppl): S21–7.

Mathis CA, Wang Y, Holt DP, Huang GF, Debnath ML, Klunk WE. Synthesis and evaluation of 11C-labeled 6-substituted 2-arylbenzothiazoles as amyloid imaging agents. J Med Chem 2003; 46: 2740–54.

Mochizuki A, Mizusawa H, Ohkoshi N, Yoshizawa K, Komatsuzaki Y, Inoue K, et al. Argentophilic intracytoplasmic inclusions in multiple system atrophy. J Neurol 1992; 239: 311–6.

Ono K, Yamada M. Antioxidant compounds have potent anti-fibrillogenic and fibril-destabilizing effects for alpha-synuclein fibrils in vitro. J Neurochem 2006; 97: 105–15.

Ozawa T, Paviour D, Quinn NP, Josephs KA, Sangha H, Kilford L, et al. The spectrum of pathological involvement of the striatonigral and olivopontocerebellar systems in multiple system atrophy: clinicopathological correlations. Brain 2004; 127: 2657–71.

Papp MI, Lantos PL. The distribution of oligodendroglial inclusions in multiple system atrophy and its relevance to clinical symptomatology. Brain 1994; 117(Pt 2): 235–43.

Sakamoto M, Uchihara T, Nakamura A, Mizutani T, Mizusawa H. Progressive accumulation of ubiquitin and disappearance of alpha-synuclein epitope in multiple system atrophy-associated glial cytoplasmic inclusions: triple fluorescence study combined with Gallyas-Braak method. Acta Neuropathol 2005; 110: 417–25.

Shy GM, Drager GA. A neurological syndrome associated with orthostatic hypotension: a clinical-pathologic study. Arch Neurol 1960; 2: 511–27.

Stefanova N, Reindl M, Neumann M, Haass C, Poewe W, Kahle PJ, et al. Oxidative stress in transgenic mice with oligodendroglial alpha-synuclein overexpression replicates the characteristic neuropathology of multiple system atrophy. Am J Pathol 2005; 166: 869–76.

Takahashi H, Wakabayashi K. Controversy: is Parkinson's disease a single disease entity? Yes. Parkinsonism Relat Disord 2005; 11(Suppl 1): S31–7.

Tashiro M, Okamura N, Furumoto S, Kumagai K, Furukawa K, Sugi K, et al. Quantitative analysis of amyloid deposition in Alzheimer's disease patients and healthy volunteers using PET and [11C]BF-227. In: Proceedings of the International Symposium on Early Detection and Rehabilitation Technology of Dementia 2009 (DRD2009). Okayama, Japan, 2009.110–1.

Tong J, Wong H, Guttman M, Ang LC, Forno LS, Shimadzu M, et al. Brain alpha-synuclein accumulation in multiple system atrophy, Parkinson's disease and progressive supranuclear palsy: a comparative investigation. Brain 2010; 133: 172–88.

van der Eecken H, Adams RD, van Bogaert L. Striopallidal-nigral degeneration. An hitherto undescribed lesion in paralysis agitans. J Neuropathol Exp Neurol 1960; 19: 159–61.

Wakabayashi K, Takahashi H. Cellular pathology in multiple system atrophy. Neuropathology 2006; 26: 338–45.

Wakabayashi K, Yoshimoto M, Tsuji S, Takahashi H. Alpha-synuclein immunoreactivity in glial cytoplasmic inclusions in multiple system atrophy. Neurosci Lett 1998; 249: 180–2.

Ye L, Velasco A, Fraser G, Beach TG, Sue L, Osredkar T, et al. In vitro high affinity alpha-synuclein binding sites for the amyloid imaging agent PIB are not matched by binding to Lewy bodies in postmortem human brain. J Neurochem 2008; 105: 1428–37.

ORIGINAL COMMUNICATION

Amyloid PET in mild cognitive impairment and Alzheimer's disease with BF-227: comparison to FDG–PET

Katsutoshi Furukawa · Nobuyuki Okamura · Manabu Tashiro · Masaaki Waragai · Shozo Furumoto · Ren Iwata · Kazuhiko Yanai · Yukitsuka Kudo · Hiroyuki Arai

Abstract We recently developed a novel PET tracer, ^{11}C-labeled 2-(2-[2-dimethylaminothiazol-5-yl]ethenyl)-6-(2-[fluoro]ethoxy)benzoxazole ([^{11}C]BF-227), and had success with in vivo detection of amyloid plaques in Alzheimer's disease (AD) brains (Kudo et al. in J Nucl Med 8:553–561, 2007). We applied this tracer to subjects with mild cognitive impairment (MCI) and AD in order to elucidate the status of amyloid plaque deposition in MCI and compared the diagnostic performance of BF-227-PET with that of FDG–PET in AD cases. We studied 12 aged normal (AN) subjects, 15 MCIs and 15 ADs with PET using [^{11}C]BF-227. PET images were obtained after administration of BF-227 and the regional standardized uptake value (SUV) and the ratio of regional to cerebellar SUV were calculated as an index of BF-227 binding. AD patients showed increased uptake of [^{11}C]BF-227 in the neocortical areas and striatum as well as decreased glucose metabolism in temporoparietal, posterior cingulate and medial temporal areas. MCI subjects showed a significant increase in BF-227 uptake in the neocortical areas similar to AD, and the most significant difference of BF-227 retention was observed in the parietal lobe if its retentions for MCI were compared to those for AD and AN. On the other hand, glucose hypometabolism in MCI was confined to cingulate and medial temporal cortices. Neocortical BF-227 uptake negatively correlated with glucose metabolism. Receiver operating characteristic (ROC) analysis indicated higher specificity and sensitivity with BF-227-PET than those with FDG–PET for differential diagnosis between AD and normal control. We conclude that [^{11}C]BF-227-PET has a possibility to be a useful technology for early detection of AD pathology and also even in the MCI stage.

Keywords Alzheimer's disease · Amyloid · Senile plaque · PET · MCI

K. Furukawa and N. Okamura equally contributed to the article.

K. Furukawa (✉) · M. Waragai · H. Arai
Department of Geriatrics and Gerontology,
Division of Brain Sciences, Institute of Development,
Aging and Cancer, Tohoku University,
4-1 Seiryomachi, Aobaku, Sendai 980-8498, Japan
e-mail: kfurukawa-ns@umin.ac.jp

N. Okamura · S. Furumoto · K. Yanai
Department of Pharmacology,
Tohoku University Graduate School of Medicine,
4-1 Seiryomachi, Aobaku, Sendai 980-8575, Japan

M. Tashiro
Division of Cyclotron Nuclear Medicine,
Cyclotron and Radioisotope Center, 6-3Aoba,
Aramaki, Aoba-ku, Sendai, Miyagi 980-8578, Japan

R. Iwata
Division of Radiopharmaceutical Chemistry,
Cyclotron and Radioisotope Center, 6-3Aoba,
Aramaki, Aoba-ku, Sendai, Miyagi 980-8578, Japan

Y. Kudo
Department of NeuroImaging Research,
Innovation New Biomedical Engineering Center,
Tohoku University, 4-1 Seiryomachi, Aobaku,
Sendai 980-8498, Japan

Introduction

Senile or amyloid plaque is a pathological hallmark of Alzheimer's disease (AD), and amyloid β peptide (Aβ), which is a main component of the senile plaque, is believed to play a key role in the pathogenesis of AD [8]. In recent years several laboratories, including ours, have succeeded in visualizing Aβ deposition in living patients' brains with

AD using PET probes [13, 14, 24]. Pittsburgh Compound-B (PIB), which is the most commonly used probe for Aβ now, has been applied not only to AD but also to several other neurological disorders [15, 24].

Petersen from the Mayo clinic addressed the concept of mild cognitive impairment (MCI), which is an intermediate state between normal aging and AD [20, 21]. The criteria he stated for MCI are cognitive concern expressed by a physician, informant, participant or nurse; cognitive impairment in one or multiple domains (executive function, memory, language or visuospatial); normal functional activities; not demented.

Regional cerebral glucose metabolism (rCMRglu) has been studied by several investigators [9, 18, 19] using [^{18}F] 2-fluoro-deoxy-D-glucose (FDG) and PET in diseases causing dementia including AD. We used BF-227-PET as well as FDG–PET on the same subjects (AN, MCI, and AD) and carefully analyzed and compared the results with these two kinds of PET. Finally using these data we investigated and compared the specificity and sensitivity of BF-227 PET and FDG–PET in diagnosing AD.

Method

Twelve ANs, 15 subjects with MCI and 15 patients with AD were recruited in the present study. The demographic information of the subjects is shown in Table 1. The diagnosis for MCI and probable AD followed the MCI clinical criteria presented by "Petersen et al." [20] and "the National Institute of Neurological and Communicative Disorders and Stroke—Alzheimer's Disease and Related Disorders Association" [17], respectively. In 15 MCI subjects, 10 were amnestic multi-domain MCI and the other 5 subjects were amnestic single-domain MCI. Mini-mental state examination (MMSE) scores were significantly different between "AN and MCI", "AN and AD", and "MCI and AD". The study protocol was approved by the Committee on Clinical Investigation at Tohoku University School of Medicine and the Advisory Committee on Radioactive Substances at Tohoku University. After a complete description of the study to the patients and subjects, written informed consent was obtained.

Table 1 Demographic details of the subjects in this study

	N	Gender	Age	MMSE
AN	12	M/F = 7/5	66.3 ± 3.3	29.9 ± 0.3
MCI	15	M/F = 8/7	78.3 ± 3.8	25.5 ± 2.5
AD	15	M/F = 5/10	72.5 ± 6.9	19.5 ± 3.7

AN aged normal, *MCI* mild cognitive impairment, *AD* Alzheimer's disease. MMSE scores are significantly different between "AN and MCI", "AN and AD", and "MCI and AD"

The PET procedure for BF-227 was described precisely before [14]. BF-227 and its N-desmethylated derivative (a precursor of [^{11}C]BF-227) were custom-synthesized by Tanabe R&D Service Co. [^{11}C]BF-227 was synthesized from the precursor by N-methylation in dimethyl sulfoxide using [^{11}C]methyl triflate. The [^{11}C]BF-227 PET study was performed using a PET SET-2400 W scanner (Shimadzu Inc., Japan). After intravenous injection of 211–366 mBq of [^{11}C]BF-227, dynamic PET images were obtained for 60 min with each subject's eyes closed. Standardized uptake value (SUV) images of [^{11}C]BF-227 were obtained by normalizing tissue radioactivity concentration by injected dose and body weight. The FDG–PET procedure was described previously [19]. Subjects were scanned in a quiet and dimly-lit room with their eyes closed after at least 4 h of food restriction. Following a 68 Ga/Ga transmission scan of 7 min duration, an emission scan, which lasted 60 min after intravenous injection of FDG, was performed. The emission data were corrected for tissue attenuation using the transmission data. Regions of interest (ROIs) were placed on individual axial magnetic resonance (MR) images in the cerebellar hemisphere, striatum, frontal, lateral temporal, medial temporal, parietal, occipital, anterior and posterior cingulate cortices. The ROI information was then copied onto dynamic PET SUV images, and regional SUVs were sampled using Dr. View/LINUX software (AJS inc., Japan). Because there were neither senile plaques nor glucose hypometabolism in the cerebellum of AD, ratios of regional SUV to cerebellar SUV (SUVR) were calculated as an index of [^{11}C]BF-227 retention and CMRglu. Neocortical SUVR was calculated by averaging SUVRs in the frontal, lateral temporal, parietal and posterior cingulate cortices.

For statistical comparison in the three groups, we applied one-way analysis of variance (ANOVA) followed by the Bonferroni-Dunn post hoc test. The performance of diagnostic indices to discriminate among groups was assessed using the ROC analysis. Areas under ROC curves (AUC) were calculated and compared using GraphPad Prism Software (GraphPad Software Inc., San Diego, CA). Statistical significance was defined as $p < 0.05$.

Results

BF-227 retention in MCI

First, we analyzed PET images with [^{11}C]BF-227 among the three groups (AN, MCI, and AD), and representative brain PET images are shown in Fig. 1. As indicated in the figure, some MCI subjects showed strong retention of [^{11}C]BF-227, but other MCI subjects did not. Most AD cases, however, indicated strong accumulation of [^{11}C]BF-227 especially in

Fig. 1 Representative axial brain PET images with BF-227. Both the AD cases showed high SUVR compared to the aged normal subjects, although the MCI cases showed heterogeneity, that is, one MCI case (MMSE = 25) showed a comparative SUVR level to AN but another case showed SUVR as high as the AD level
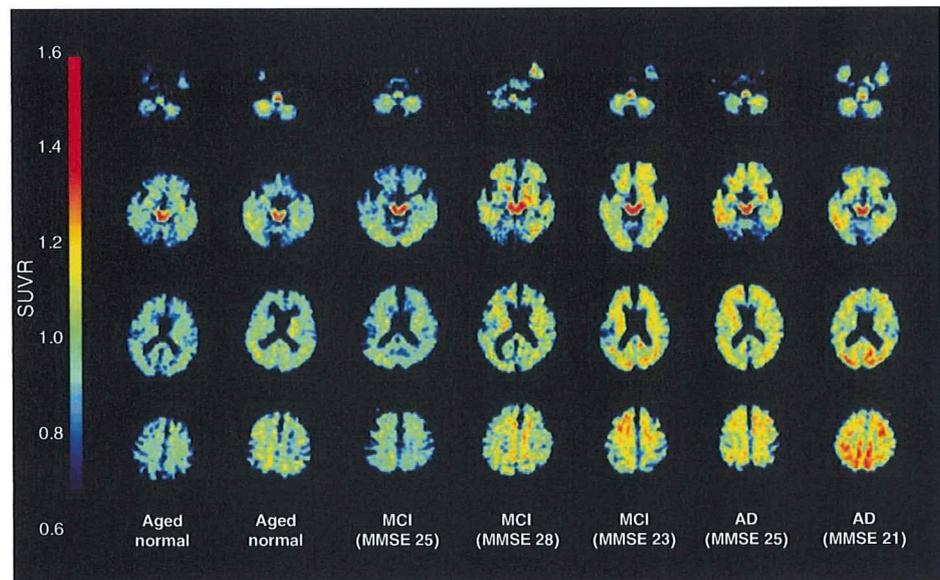
frontal, temporal and parietal cortices. If the retention pattern of [^{11}C]BF-227 is compared to that of PIB, the accumulation of [^{11}C]BF-227 in the frontal lobe looks much weaker than that of PIB [3].

Figure 2 shows the mean neocortical and regional SUVRs of [^{11}C]BF-227 for the three groups. Both the mean neocortical SUVRs for MCI and AD are significantly higher than that for AN. As we previously reported [1], significantly higher SUVRs were observed in most cerebral regions in AD compared to AN except for the medial temporal lobe. MCI subjects indicated a significantly increased SUVR in frontal, lateral temporal, parietal, occipital cortices as well as anterior cingulate gyrus compared to AN, and the most prominent increase was observed in the lateral temporal cortex. A significantly lower SUVR in MCI was observed in the parietal cortex compared to AD. In the other neocortical regions, MCI subjects showed a tendency towards milder retention of BF-227 than that in AD. In the relationship between BF retentions and MMSE scores in all the subjects together (NC, MCI, and AD), no strong correlations were observed (data not shown).

Cerebral glucose metabolism in AN, MCI and AD

Next, we analyzed CMRglu in the same subjects using FDG–PET in order to compare to the findings with [^{11}C]BF-227, which is considered to indicate amyloid plaque depositions. As a result, a significant reduction of neocortical SUVR was observed in both MCI and AD patients compared to AN in FDG–PET (Table 1; Fig. 3). Regional SUVR in FDG–PET was significantly decreased in the cingulate gyrus and medial temporal cortex of MCI

subjects and in the lateral temporal, parietal, posterior cingulate and medial temporal cortices of AD patients, compared to AN. Table 2.

Neocortical SUVR of FDG–PET for each subject was plotted against neocortical SUVR of BF-227-PET (Fig. 4a). SUVR of BF-227 negatively correlated to SUVR of FDG in analyzing the subjects from three groups all together ($r = -0.337$, $p = 0.029$). A significant correlation of regional SUVR in BF-227-PET and FDG–PET was also observed in the temporal and parietal cortices (data not shown). However, no significant correlation was observed when the analysis was confined to the subjects in each group.

Furthermore, in order to compare sensitivity and specificity to differentiate AD from AN, ROC analysis was performed for the lateral temporal SUVR of BF-227 and posterior cingulate SUVR of FDG (Fig. 4b). The AUC for BF-227 (0.994) is much higher than that for FDG (0.839), indicating that BF-227 is more sensitive as well as more specific than FDG in diagnosing AD.

Discussion

Our group recently developed a novel PET tracer, BF-227, and has reported that this compound is able to selectively detect dense amyloid deposits including senile plaques primarily in the posterior association area of AD patients. In the present study we applied this tracer to MCI cases and concluded that the mean value for the MCI cases with BF-227 was intermittent between AN and AD. Also we clarified that BF-227-PET is a useful technology to distinguish early AD patients from AN compared to FDG–PET.

Fig. 2 Box plots of SUVR values with BF-227 PET for AN, MCI and AD. Each *dot* indicates the mean SUVR from "the mean neocortex" and "the eight regions", that is, frontal, temporal, parietal, occipital, anterior cingulate, posterior cingulated, striatum and medial temporal cortex. *Box* indicates interquartile range. *Vertical bars* indicate minimum–maximum range
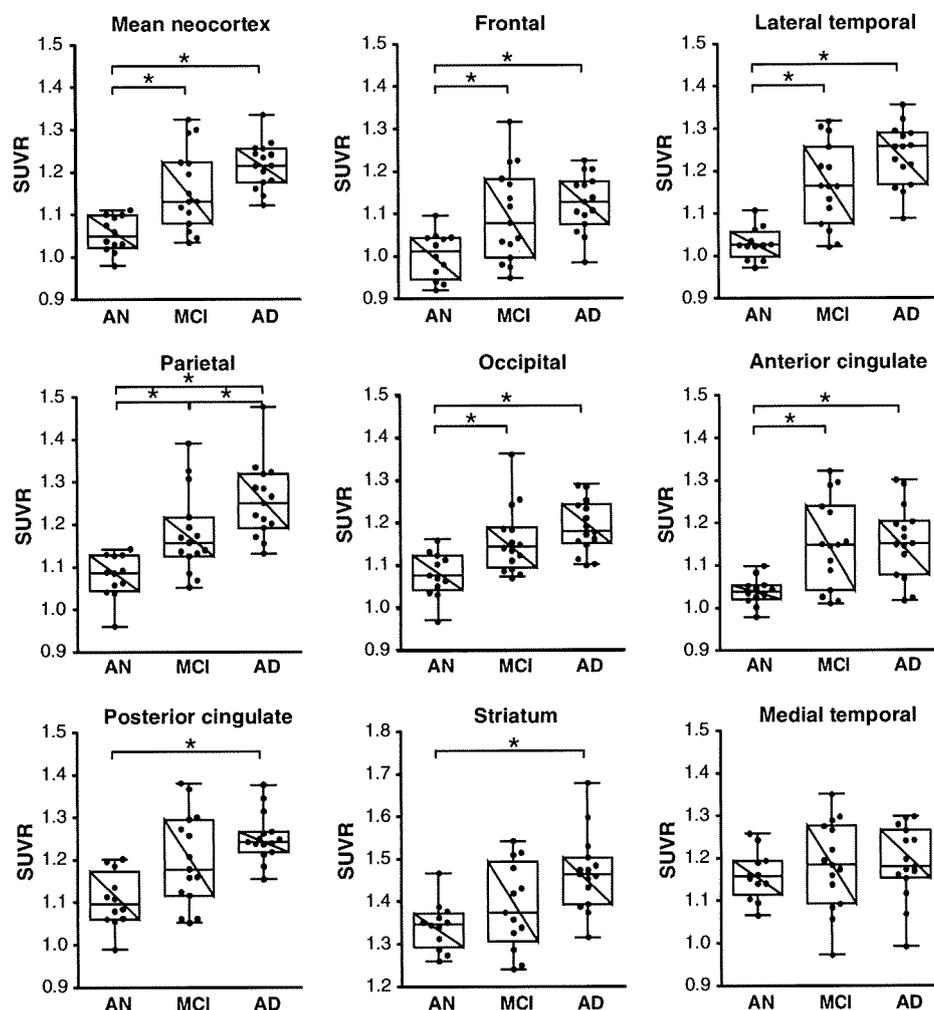
MCI is now classified into 4 subtypes, that is, amnestic single-domain MCI, amnestic multi-domain MCI, non-amnestic single-domain MCI and non-amnestic multi-domain MCI. The important thing is that MCI (especially amnestic MCI) is regarded as a prodromal state of AD, in other words, a high percentage of MCI subjects are considered to convert to AD. It has been reported that 10–20% of MCI cases are going to convert to AD although only 1–2% of normal elderly convert to AD [21]. The present study concludes that MCI has high levels of [11C]BF-227 retention indicating that senile plaque deposition already advances severely in the stage of MCI before dementia symptoms become obvious. Previous amyloid PET studies using ^{18}F-labeled 2-(1,1-dicyano-propen-2-yl)-6-(2-fluoroethyl)-methylamino-naphthalene (FDDNP) or PIB also indicated significant tracer retention in MCI and AD. Small et al. [24] presented that FDDNP can detect a high signal in MCI by binding not only for amyloid plaques but also tau neurofibrillary tangles, and

the retention level for MCI is between AN and AD. On the other hand, several groups reported that about a half of the MCI subjects showed PIB uptake in the AD range, and other MCI subjects indicated retention levels lower than the AD range [12]. A group from Sweden concluded that MCI subjects who converted to AD later showed significantly higher PIB retention compared to non-converting MCI subjects and NC [6]. The present study also revealed higher retention of BF-227 in 60–70% of MCI subjects and in almost all the AD patients. Therefore, the amyloid PET technique is considered to be a highly useful and strong method for early detection of AD patients in the MCI stage. These pieces of information are indispensable in applying new treatment technologies against dementia into the prodromal stage of Alzheimer's disease. In other words, because it is considered that aggregation and deposition of Aβ starts much earlier before patients indicate symptoms of dementia, it is undoubtedly important to detect Aβ deposition as early as

Fig. 3 Box plots of SUVR values with FDG–PET for AN, MCI and AD. Each *dot* indicates the mean SUVR from the mean neocortex and eight cerebral regions, that is, frontal, temporal, parietal, occipital, anterior cingulate, posterior cingulated, striatum and medial temporal cortex. *Boxes* indicate interquartile range. *Vertical bars* indicate minimum–maximum range
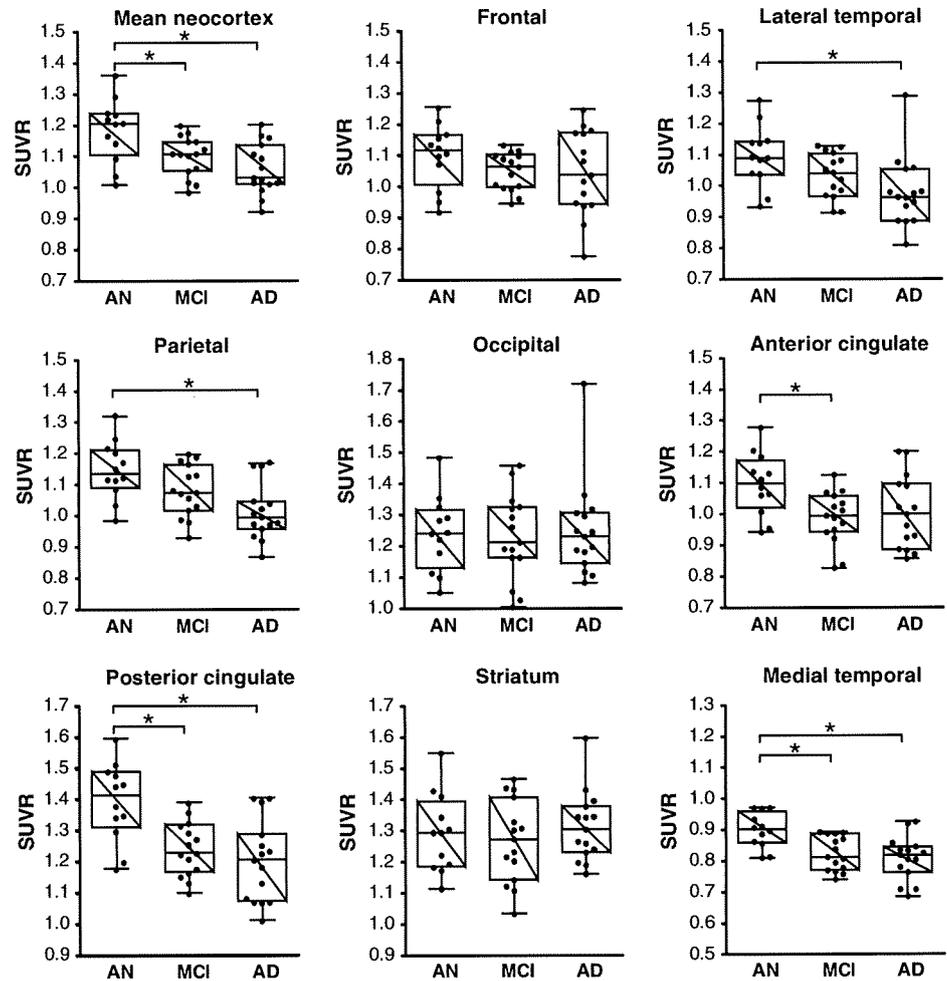

Table 2 Comparison of SUVR values of BF-227-PET and FDG–PET

		Mean neo cortex	Frontal	Lateral temporal	Parietal	Occipital	Anterior cingulate	Posterior cingulate	Striatum	Medial temporal
BF-227	AN	1.05 ± 0.04	1.00 ± 0.06	1.03 ± 0.04	1.08 ± 0.05	1.08 ± 0.05	1.04 ± 0.03	1.11 ± 0.07	1.34 ± 0.06	1.16 ± 0.06
	MCI	1.16 ± 0.10*	1.10 ± 0.11*	1.17 ± 0.10*	1.18 ± 0.10*	1.16 ± 0.08*	1.15 ± 0.11*	1.20 ± 0.11	1.41 ± 0.11	1.18 ± 0.10
	AD	1.22 ± 0.06*	1.13 ± 0.07*	1.24 ± 0.07*	1.25 ± 0.09*†	1.19 ± 0.06*	1.16 ± 0.09*	1.25 ± 0.06*	1.47 ± 0.09*	1.19 ± 0.09
FDG	AN	1.18 ± 0.10	1.10 ± 0.11	1.10 ± 0.10	1.15 ± 0.09	1.24 ± 0.12	1.10 ± 0.10	1.39 ± 0.13	1.29 ± 0.13	0.90 ± 0.06
	MCI	1.10 ± 0.06*	1.05 ± 0.06	1.03 ± 0.07	1.08 ± 0.08	1.23 ± 0.14	0.99 ± 0.08*	1.24 ± 0.09*	1.27 ± 0.13	0.82 ± 0.06*
	AD	1.06 ± 0.08*	1.05 ± 0.14	0.98 ± 0.11*	1.01 ± 0.09*	1.25 ± 0.15	1.00 ± 0.12	1.20 ± 0.13*	1.31 ± 0.11	0.81 ± 0.07*

Mean SUVR value for each brain region was obtained from AN, MCI and AD. * $p < 0.05$, versus AN, † $p < 0.05$ versus MCI

possible in order to begin medication to prevent or treat cognitive decline before the manifestations of dementia become clear.

In most PIB positive MCI and AD cases presented by several different laboratories, the frontal cortex showed high PIB retention, although the frontal cortex is not a region where amyloid plaques are predominantly rich in the early stage of AD or MCI according to the autopsy studies [1, 10]. Our newly developed tracer, BF-227, showed relatively high retention in temporal and parietal lobes for MCI and AD compared to the results with PIB. Since it is well known that the functional activity of the parietal lobe decreases in the early stage of AD [16], it is reasonable that the distribution of high BF-227-PET
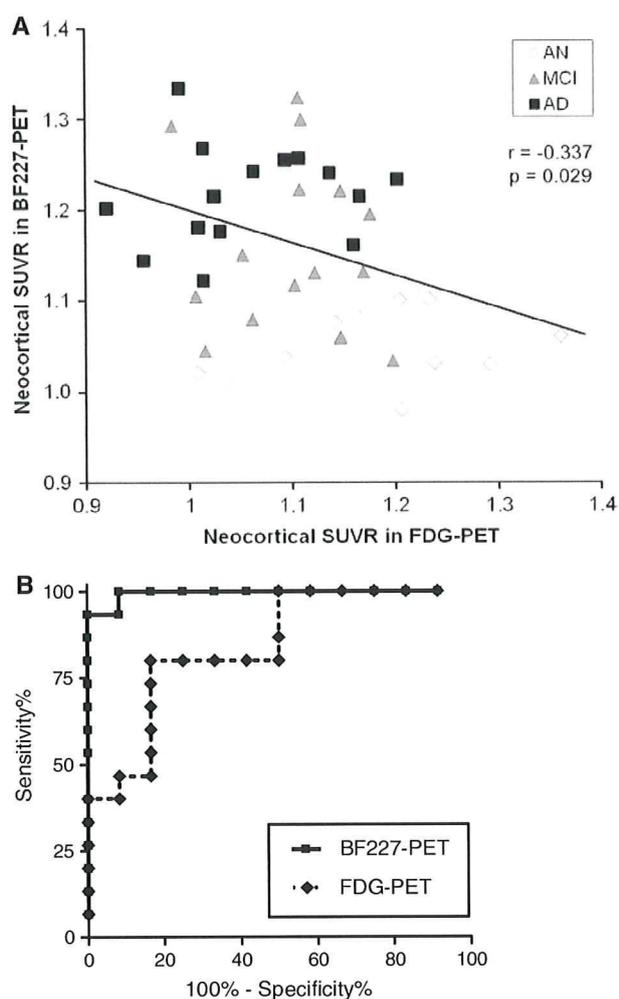
Fig. 4 **a** Relationship between neocortical SUVRs in FDG–PET and BF-227-PET. Neocortical SUVR of FDG–PET for each subject was plotted against neocortical SUVR of BF-227-PET. White, gray and black dots indicate AN, MCI and AD, respectively. **b** Receiver operating characteristic (ROC) curves of BF-227 and FDG–PET. BF-227-PET SUVR in the lateral temporal cortex and FDG–PET SUVR in the posterior cingulate cortex for differentiation between AD and AN

retention is closely related to the area indicating functional deterioration in the early stage of AD or MCI.

Low rCMRglu in AD especially in the posterior cingulate, precuneus, temporoparietal and frontal cortices was reported. FDG–PET has also been used in investigations for MCI, and low rCMRglu in the temporo-parietal and medial frontal cortices and hippocampus was reported as the most prominent predictor of subsequent cognitive decline [2–5]. Our results indicate, however, that amyloid retention detected by BF-227 is more sensitive and specific than FDG–PET for AD diagnosis. Therefore it is reasonable that amyloid PET is more sensitive than FDG–PET for detecting MCI, which is regarded as a prodromal state of

dementia or early AD. According to previous autopsy studies with MCI, amyloid plaques were found predominantly in the temporal lobe structure and most amnestic MCI cases showed Braak stage II or III [11, 22]. Furthermore both neurofibrillary tangles and senile plaques were found in nondemented aging and "preclinical" AD, and profound neuronal loss was observed in layer II of the entorhinal cortex [7, 23]. Our results with BF-227 PET for MCI presented here agree with postmortem studies because BF-227 also showed high retention predominantly in the temporal lobe and the retention was intermittent between NC and AD. There are some discrepancies, however, between the results with our BF-227-PET and with autopsy, that is, some cerebral white matter, thalamus and pons showed high retention of BF-227 in MCI, although these regions are usually not rich in senile plaques in the autopsy studies. Although it is considered that the deposition of BF-227 in these regions comes from its non-specific retention by high lipophilicity, it is supposed that more precise studies are needed using more subjects for both PET and autopsy.

We now have to carefully consider the heterogeneity of BF-227 retention in MCI, which was also observed in FDDNP or PIB studies, that is, some subjects show rich retention but others do not. Although it was reported that MCI subjects showing high retention of PIB had a high tendency to convert to AD as we mentioned above [6], the number of subjects they examined was relatively small. Therefore, further careful studies are needed to clarify if the accumulation of amyloid PET probes correlates with the severity of cognitive impairment and a conversion rate to dementia.

Our results using BF-227 for MCI are "continuous" rather than "off/on", "negative/positive" or "dichotomous" signals compared to those with PIB. We speculate that because BF-227 can depict a small difference of amyloid deposition more finely than PIB, the results with BF-227 in MCI are more continuous than those with PIB. Therefore, BF-227 could reveal a degree of senile plaque deposition more precisely and accurately than PIB as far as in cases with MCI.

We would like to conclude that our newly developed amyloid PET tracer, BF-227, can detect amyloid aggregation and deposition in MCI cases and the PET signal intensity for MCI was intermittent between NC and AD. Results obtained with BF-227 PET are significantly more sensitive and specific than FDG–PET in diagnosing AD. As far as the retention pattern in the frontal and parietal cortices, BF-227 more accurately reflects senile plaque deposition observed in the autopsy studies than PIB does. Therefore, BF-227 PET should be an invaluable tool for diagnosis of AD in the early stage. Finally, we recently developed a novel probe, which has similar structure to BF-

227, labeled with F-18, and applied it to living humans. We have finished more than 20 cases so far and obtained similar results to BF-227.

References

1. Bennett DA, Cochran EJ, Saper CB, Leverenz JB, Gilley DW, Wilson RS (1993) Pathological changes in frontal cortex from biopsy to autopsy in Alzheimer's disease. Neurobiol Aging 14:589–596
2. Chételat G, Desgranges B, de la Sayette V, Viader F, Eustache F, Baron JC (2003) Mild cognitive impairment: Can FDG-PET predict who is to rapidly convert to Alzheimer's disease? Neurology 60:1374–1377
3. Chételat G, Eustache F, Viader F, De La Sayette V, Pélerin A, Mézenge F, Hannequin D, Dupuy B, Baron JC, Desgranges B (2005) FDG–PET measurement is more accurate than neuropsychological assessments to predict global cognitive deterioration in patients with mild cognitive impairment. Neurocase 11:14–25
4. de Leon MJ, Convit A, Wolf OT, Tarshish CY, DeSanti S, Rusinek H, Tsui W, Kandil E, Scherer AJ, Roche A, Imossi A, Thorn E, Bobinski M, Caraos C, Lesbre P, Schlyer D, Poirier J, Reisberg B (2001) Fowler et al. Prediction of cognitive decline in normal elderly subjects with 2-[(18)F]fluoro-2-deoxy-D-glucose/positron-emission tomography (FDG/PET). Proc Natl Acad Sci USA 98:10966–10971
5. Drzezga A, Lautenschlager N, Siebner H, Riemenschneider M, Willoch F, Minoshima S, Schwaiger M, Kurz A (2003) Cerebral metabolic changes accompanying conversion of mild cognitive impairment into Alzheimer's disease: a PET follow-up study. Eur J Nucl Med Mol Imaging 30:1104–1113
6. Forsberg A, Engler H, Almkvist O, Blomquist G, Hagman G, Wall A, Ringheim A, Långström B, Nordberg A (2008) A PET imaging of amyloid deposition in patients with mild cognitive impairment. Neurobiol Aging 29:1456–1465
7. Gómez-Isla T, Price JL, McKeel DW Jr, Morris JC, Growdon JH, Hyman BT (1996) Profound loss of layer II entorhinal cortex neurons occurs in very mild Alzheimer's disease. J Neurosci 16:4491–4500
8. Hardy J, Selkoe DJ (2002) The amyloid hypothesis of Alzheimer's disease: progress and problems on the road to therapeutics. Science 297:353–356
9. Herholz K, Carter SF, Jones M (2007) PET studies in dementia. Br J Radiol 80:S160–S167
10. Iwatsubo T, Odaka A, Suzuki N, Mizusawa H, Nukina N, Ihara Y (1994) Visualization of A beta 42(43) and A beta 40 in senile plaques with end-specific A beta monoclonals: evidence that an initially deposited species is A beta 42(43). Neuron 13:45–53
11. Jicha GA, Parisi JE, Dickson DW, Johnson K, Cha R, Ivnik RJ, Tangalos EG, Boeve BF, Knopman DS, Braak H, Petersen RC (2006) Neuropathologic outcome of mild cognitive impairment following progression to clinical dementia. Arch Neurol 63:674–681
12. Kemppainen NM, Aalto S, Wilson IA, Någren K, Helin S, Brück A, Oikonen V, Kailajärvi M, Scheinin M, Viitanen M, Parkkola R, Rinne JO (2007) PET amyloid ligand [11C]PIB uptake is increased in mild cognitive impairment. Neurology 68:1603–1606
13. Klunk WE, Engler H, Nordberg A, Wang Y, Blomqvist G, Holt DP, Bergström M, Savitcheva I, Huang GF, Estrada S, Ausén B, Debnath ML, Barletta J, Price JC, Sandell J, Lopresti BJ, Wall A, Koivisto P, Antoni G, Mathis CA, Långström B (2004) Imaging brain amyloid in Alzheimer's disease with Pittsburgh Compound-B. Ann Neurol 55:306–319
14. Kudo Y, Okamura N, Furumoto S, Tashiro M, Furukawa K, Maruyama M, Itoh M, Iwata R, Yanai K, Arai H (2007) 2-(2-[2-Dimethylaminothiazol-5-yl]ethenyl) -6-(2-[fluoro]ethoxy)benzoxazole: a novel PET agent for in vivo detection of dense amyloid plaques in Alzheimer's disease patients. J Nucl Med 8:553–561
15. Mathis CA, Klunk WE, Price JC, DeKosky ST (2005) Imaging technology for neurodegenerative diseases: progress toward detection of specific pathologies. Arch Neurol 62:196–200
16. Matsuda H (2007) Role of neuroimaging in Alzheimer's disease, with emphasis on brain perfusion SPECT. J Nucl Med 48:1289–1300
17. McKhann G, Drachman D, Folstein M, Katzman R, Price D, Stadlan EM (1984) Clinical diagnosis of Alzheimer's disease: report of the NINCDS-ADRDA Work Group under the auspices of Department of Health and Human Services Task Force on Alzheimer's Disease. Neurology 34:939–944
18. Minoshima S, Giordani B, Berent S, Frey KA, Foster NL, Kuhl DE (1997) Metabolic reduction in the posterior cingulate cortex in very early Alzheimer's disease. Ann Neurol 42:85–94
19. Okamura N, Arai H, Higuchi M, Tashiro M, Matsui T, Hu XS, Takeda A, Itoh M, Sasaki H (2001) [18F]FDG–PET study in dementia with Lewy bodies and Alzheimer's disease. Prog Neuropsychopharmacol Biol Psychiatry 25:447–456
20. Petersen RC, Smith GE, Waring SC, Ivnik RJ, Tangalos EG, Kokmen E (1999) Mild cognitive impairment: clinical characterization and outcome. Arch Neurol 56:303–308
21. Petersen RC (2004) Mild cognitive impairment as a diagnostic entity. J Intern Med 256:183–194
22. Petersen RC, Parisi JE, Dickson DW, Johnson K, Cha R, Ivnik RJ, Tangalos EG, Boeve BF, Knopman DS, Braak H, Petersen RC (2006) Neuropathologic features of amnestic mild cognitive impairment. Arch Neurol 63:665–672
23. Price JL, Morris JC (1999) Tangles and plaques in nondemented aging and "preclinical" Alzheimer's disease. Ann Neurol 45:358–368
24. Small GW, Kepe V, Ercoli LM, Siddarth P, Bookheimer SY, Miller KJ, Lavretsky H, Burggren AC, Cole GM, Vinters HV, Thompson PM, Huang SC, Satyamurthy N, Phelps ME, Barrio JR (2006) PET of brain amyloid and tau in mild cognitive impairment. N Engl J Med 355:2652–2663
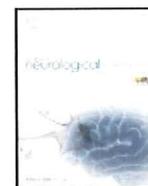
Comparison study of amyloid PET and voxel-based morphometry analysis in mild cognitive impairment and Alzheimer's disease

Masaaki Waragai [a], Nobuyuki Okamura [b,*], Katsutoshi Furukawa [a], Manabu Tashiro [c], Shozo Furumoto [b,d], Yoshihito Funaki [e], Motohisa Kato [b], Ren Iwata [e], Kazuhiko Yanai [b], Yukitsuka Kudo [f], Hiroyuki Arai [a]

[a] Department of Geriatrics and Gerontology, Division of Brain Sciences, Institute of Development, Aging and Cancer, Tohoku University, Sendai, Japan
[b] Department of Pharmacology, Tohoku University School of Medicine, Sendai, Japan
[c] Division of Cyclotron Nuclear Medicine, Cyclotron and Radioisotope Center, Tohoku University, Sendai, Japan
[d] Department of Nuclear Medicine and Radiology, Institute of Development, Aging and Cancer, Tohoku University, Sendai, Japan
[e] Division of Radiopharmaceutical Chemistry, Cyclotron and Radioisotope Center, Tohoku University, Sendai, Japan
[f] Innovation of New Biomedical Engineering Center, Tohoku University, Sendai, Japan

ABSTRACT

Two techniques employed for the early diagnosis of dementia are the imaging of amyloid-β protein using positron emission tomography (PET) and voxel-based morphometry analysis of MRI (VBM–MRI). The purpose of this study was to evaluate the clinical utility of amyloid PET and VBM–MRI for the early diagnosis and tracking of the severity of Alzheimer's disease (AD). The neuritic plaque burden and gray matter losses were evaluated using [^{11}C]BF-227–PET and VBM–MRI in 12 healthy controls, 13 subjects with mild cognitive impairment (MCI), including 6 who converted to AD and 7 who did not convert, and 15 AD patients. The AD patients and the MCI converters exhibited a neocortical retention of BF-227 and parahippocampal gray matter loss shown by VBM–MRI. The MCI converters were more clearly distinguished from the MCI non-converters in BF-227–PET than VBM–MRI. The combined sample of the MCI converters and AD patients showed a significant correlation of MMSE scores with the global gray matter loss, but not with the BF-227 retention. These findings suggest that amyloid PET using [^{11}C]BF-227 is better suited for the prediction of conversion from MCI to AD, while VBM–MRI appears to be better suited for tracking the severity of dementia.

© 2009 Elsevier B.V. All rights reserved.

1. Introduction

Alzheimer's disease (AD) is a neurodegenerative disorder characterized by a progressive impairment of cognitive function and behavior. AD is the most common form of dementia, particularly in the elderly [1,2]. The pathological hallmarks of AD are extracellular amyloid-β protein deposits called senile plaques (SPs) and intracellular neurofibrillary tangles (NFTs), which occur together with selective neuronal and synaptic loss [3,4]. These changes are also associated with progressive neuronal loss and resultant cerebral atrophy [5]. The presence of both SPs and NFTs are prerequisites for a definitive diagnosis of AD, but more attention has been focused on the role of amyloid-β protein (Aβ) in the pathogenesis of AD. Although the mechanisms of development of AD have not been completely elucidated, Aβ is assumed to play a causal role in the pathology of AD.

In vivo imaging techniques that can non-invasively and reliably assess Aβ deposition are currently receiving considerable attention in the search for a method for early diagnosis of AD [6–11]. Pittsburgh Compound-B (PIB) is at present the most commonly used probe for Aβ and has been applied to the diagnosis of AD and several other neurological disorders [12–16]. For example, amnesic mild cognitive impairment (MCI) is currently considered a prodromal state of AD, though not all individuals with MCI will develop AD; MCI converters and non-converters are difficult to distinguish from a clinical and neuropsychological perspective. Analysis of PIB–PET images in MCI subjects revealed a bimodal distribution of PIB uptake in the neocortex. About two thirds of MCI cases showed neocortical retention of PIB similar in distribution (and sometimes in degree) to AD, while the other third of MCI cases showed no cortical retention, similar to normal individuals [15,17,18]. A previous PIB–PET study demonstrated higher PIB retention in MCI converters than in non-converters, suggesting the utility of amyloid imaging in the prediction of progression to dementia [18].

We have developed novel benzoxazole derivatives for in vivo imaging of amyloid [19–21]. One of these agents, 2-(2-[2-demethylaminothiazol-5-yl]ethenyl)-6-(2-[Fluoro]ethoxy)benzoxazole (BF-227), displayed a high binding affinity to Aβ fibrils, excellent brain uptake and specifically labels amyloid deposits in transgenic mice [20,22]. A clinical PET study using [^{11}C]BF-227 demonstrated higher retention of this tracer in the

* Corresponding author. Department of Pharmacology, Tohoku University School of Medicine, Tohoku University, 2-1 Seiryo-machi, Aoba-ku, Sendai 980-8575, Japan. Tel.: +81 22 717 8058; fax: +81 22 717 8060.
E-mail address: oka@mail.tains.tohoku.ac.jp (N. Okamura).

neocortex of AD patients than normal individuals [22]. There are several drawbacks to the use of this tracer, including its relatively low affinity to AD brain tissue ($K_d = 25$ nM) compared to PIB [23] and its slower clearance from the white matter region due to its higher lipophilicity (Log$P = 1.75$),[22] resulting in lower signal to background ratio than PIB–PET. However, the voxel-based analysis of BF-227–PET images indicated a pattern of tracer distribution distinct from that of PIB–PET.[12] Intriguingly, the preferential [^{11}C]BF-227 retention in the posterior neocortical region of the AD brain corresponded with an area containing a high density of neuritic plaques [4,22]. A preliminary report of the direct comparison of PIB–PET and BF-227–PET in the same AD patients additionally demonstrated a difference in the regional distribution of these two agents, which presumably reflects their different preference for various conformations of Aβ in the senile plaque generation process [24]. From these findings, we speculate that BF-227 detects neuritic plaques containing dense amyloid fibrils preferentially, compared to PIB–PET, and provides unique information about the Aβ pathology in AD patients. The early detection of Aβ deposition is important to begin medication to prevent a cognitive decline in the stage of MCI, since it appears that the deposition of Aβ starts earlier than the clinical diagnosis of dementia [25–27]. Approximately 20–30% of healthy, age-matched subjects exhibited neocortical retention of PIB, predominantly in the prefrontal and posterior cingulate cortices [15,16]. The demonstration of PIB retention in a proportion of normal individuals supports postmortem observations that Aβ aggregation predominantly occurs before the onset of dementia. However, there is currently no evidence that all PIB-positive normal individuals are destined to develop dementia. Highly sensitive detection of Aβ leads to a potential risk for misjudging the process of normal physiological aging as a pathological indicator of AD. The accurate prediction of AD progression is thus necessary to prevent the administration of non-essential treatments to individuals who are not at risk of converting to AD. In particular, a shift of brain Aβ from the soluble to fibrillar form is closely associated with onset of AD [28]. Thus, selective detection of dense amyloid fibrils would be advantageous to differentiate normal aging process from AD with high specificity, as the deposition of neuritic plaques is strongly associated with the earliest symptoms of AD [25]. Based on this background evidence, we anticipated that BF-227–PET would more accurately predict the conversion from MCI to AD than other imaging techniques.

Cognitive decline is reported to strongly correlate with cortical atrophy in AD, suggesting that cortical degeneration is the primary basis of cognitive decline in AD [5]. Thus, an increased rate of cerebral atrophy, as evaluated using MRI, is a diagnostic feature of AD that correlates with the clinical stage/severity and is thought to represent the macroscopic consequences of neuronal destruction [29–31]. Medial temporal lobe atrophy, as seen in MRI scans of AD patients, is a sensitive marker of AD even in its earliest stages. Volumetric analysis of the entorhinal cortex distinguished subjects who were destined to develop dementia from normal controls with high accuracy [32]. However, this approach is time-consuming and highly dependent on analyst expertise because it requires accurate manual outlining of the region of interest for the measurement. Voxel-based morphometry (VBM) has emerged as an ideal tool to visualize the changes in gray matter density in disease states. This technique has been reported to detect gray matter loss in MCI and AD patients. In addition, lower gray matter density has been reported in MCI converters compared with MCI non-converters [33–37]. These findings suggest that measurement of gray matter loss in the medial temporal lobe or the other regions might predict progression from MCI to AD with high accuracy. A direct comparison of MRI with PIB–PET was previously performed in the control, MCI and AD populations [38]. The distributions of hippocampal volume did not overlap between AD and normal control groups with the exception of one control subject, and MCI subjects are evenly distributed between the AD and normal controls. In contrast, PIB–PET uptake showed a

bimodal distribution. While all AD subjects are tightly clustered in the high PIB retention range, both the normal control and MCI subjects segregate themselves into high and low PIB retention groups. The voxel-by-voxel comparisons of AD versus control patients revealed differences in the topographical distribution of amyloid deposition and in grey matter loss, suggesting that these two imaging strategies provide complementary information about AD pathology.

In this study, we performed amyloid-imaging PET using [^{11}C]BF-227 and VBM analysis of MRI images in subjects with MCI and AD. We investigated whether changes in BF-227 uptake and gray matter density were associated with later conversion to AD in MCI populations. Moreover, we examined the association of these measurements with cognitive function in AD and MCI converters to investigate whether these imaging strategies can track the severity of AD pathology.

2. Materials and methods

2.1. Staining of senile plaques using BF-227

Postmortem brain tissue from a 69-year-old male with autopsy-confirmed AD was obtained from Fukushimura Hospital (Toyohashi, Japan). Experiments were performed under the regulations of the hospital ethics committee. Serial sections (6 μm) taken from paraffin-embedded blocks of the temporal cortex were prepared in xylene and ethanol. Before BF-227 staining, quenching of autofluorescence was performed. The quenched tissue section was immersed in 100 μM of BF-227 containing 50% ethanol for 10 min. The section stained with BF-227 was then dipped briefly into water and rinsed in PBS for 60 min before coverslipping with FluorSave Reagent (Calbiochem, La Jolla, CA), and examined using an Eclipse E800 microscope (Nikon, Tokyo, Japan) equipped with a V-2A filter set (excitation 380–420 nm, dichroic mirror 430 nm, long pass filter 450 nm). An adjacent section was immunostained using a monoclonal antibody (mAb) against Aβ (6F/3D; Dako A/S, Glostrup, Denmark). After pretreatment with 90% formic acid for 5 min, sections were immersed in blocking solution for 30 min and then incubated for 60 min at 37 °C with 6F/3D at a dilution of 1:50. After incubation, sections were processed with the avidin–biotin method using a Pathostain ABC-POD(M) Kit (Wako, Osaka, Japan) and diaminobenzidine tetrahydrochloride.

2.2. Subjects

Patients recruited in the present study included 12 normal age-matched controls, 13 subjects with amnestic MCI, and 15 patients with AD. Diagnoses of probable AD were based on criteria from the National Institute of Neurological and Communicative Disorders and Stroke and the Alzheimer's Disease Related Disorders Association (NINCDS-ADRDA) [39]. The diagnosis of amnestic MCI was made according to the published criteria described previously [40]. All MCI subjects underwent medical and neuropsychological reevaluation at approximately 3 month intervals. Conversion to AD was diagnosed when (1) signs of deterioration of the general cognitive function were present and continued for at least 6 months, and (2) the patient's score on the Clinical Dementia Rating changed by more than 0.5 points. The MCI subjects were divided into two groups, MCI converters ($n = 6$) and MCI non-converters ($n = 7$). The MCI converters were defined as patients who eventually developed AD within a mean follow-up of 27.0 ± 7.9 months (range 14–30 months). The MCI non-converters were defined as having a transient memory loss or remaining cognitively stable through at least a 2 year follow-up (27.7 ± 2.2 months; range 25–30 months). The control group was recruited from volunteers who were not taking centrally-acting medications, had no cognitive impairment and had no cerebrovascular lesions identified via MRI. All subjects were screened using a questionnaire and medical history, and subjects with medical conditions potentially affecting the central nervous system were excluded. In addition, none

Table 1
Demographic characteristics of the subjects.

	Control	MCI non-converter	MCI converter	AD
N	12	7	6	15
Age (year)	67.3 ± 2.7	77.6 ± 3.1	80.2 ± 4.1	71.0 ± 5.1
Gender (F/M)	6/6	2/5	4/2	8/7
MMSE	29.9 ± 0.3	26.3 ± 1.1	25.7 ± 2.0	19.8 ± 3.5

of the subjects had asymptomatic cerebral infarction detected via T2-weighted MRI. Demographic data for the subjects are shown in Table 1. Although the MCI converters and non-converters were statistically older than the control subjects and the AD patients, no statistical difference in age was observed between the MCI converters and the non-converters. The AD patients showed a significantly lower MMSE score than the MCI converters, non-converters, and control subjects ($p < 0.05$), however, no statistical difference in MMSE score was observed between the MCI converters and the non-converters. The Committee on Clinical Investigation at Tohoku University School of Medicine and the Advisory Committee on Radioactive Substances at Tohoku University approved the study protocol.

3. MRI methods

All subjects underwent MRI with a 1.5 T MR scanner (GE Signa Hispeed, Milwaukee, WI). A three-dimensional volumetric acquisition of a T1-weighted gradient echo sequence produced a gapless series of thin axial sections using a vascular TOF SPGR sequence (echo time/repetition time, 2.4/50 ms; flip angle, 45°; acquisition matrix, 256 × 256; 1 excitation; field of view, 22 cm; slice thickness, 2.0 mm). Cerebral atrophy was evaluated by VBM [41]. For spatial normalization, a 12-parameter affine transformation was used to avoid segmentation errors caused by the partial-volume effects inherently created by warping. The normalized MRI was then segmented into gray matter, white matter, cerebrospinal fluid, and other components using SPM2 or SPM5 software. The segmentation procedure involved calculating the Bayesian probability of each voxel belonging to each tissue class based on a priori MRI information with a non-uniformity correction. The segmented gray matter images were then subjected to affine and non-linear spatial normalization using a template of a priori gray matter. The spatially normalized gray matter images were smoothed with an isotropic Gaussian kernel (12 mm at full width at half maximum) using the partial-volume effects to create a spectrum of gray matter intensities. The resulting gray matter intensities were equivalent to the weighted average of gray matter voxels located in the volume fixed by the smoothing kernel. Regional intensities can thus be considered equivalent to gray matter concentration. Differences of gray matter intensities between groups were assessed using a t-test with a height threshold of $p < 0.05$, corrected for multiple comparisons by the family-wise error method. The extent threshold was set to 100 voxels. Parahippocampal gray matter density was additionally evaluated by calculating the average intensities in the bilateral parahippocampal region of interest (ROI) using Dr.View/LINUX software (AJS, Japan). To evaluate global atrophy, a Z-score map was created via the comparison of individual gray matter images with the mean and S.D. of gray matter images of healthy controls after voxel normalization to global mean intensities. The degree of global atrophy (% global atrophy) was calculated as a ratio of the area in which the Z-score of the voxel was more than 2.0 to whole brain area, using Voxel-Based Specific Regional Analysis System for AD (VSRAD) software (Eisai, Tokyo, Japan) [42].

3.1. PET procedure

Radiosynthesis of [^{11}C]BF-227 and the procedure used for BF-227–PET were performed as described previously. [22] BF-227 and

its N-desmethylated derivative (a precursor of [^{11}C]BF-227) were custom-synthesized by Tanabe R&D Service Co. [^{11}C]BF-227 was synthesized from its precursor by N-methylation in dimethyl sulfoxide using [^{11}C]methyl triflate. The [^{11}C]BF-227–PET study was performed using a PET SET-2400W scanner (Shimadzu Inc., Japan). After an intravenous injection of 211–366 mBq [^{11}C]BF-227, dynamic PET images were obtained for 60 min with the subject's eyes closed. Standardized uptake value (SUV) images of [^{11}C]BF-227 were obtained by normalizing the tissue radioactivity concentration to the injected dose and body weight. ROIs were placed on individual axial MR images in the cerebellar hemisphere and the frontal, lateral temporal, parietal and posterior cingulate cortices. The ROI information was then copied onto the dynamic PET SUV images, and regional SUVs were sampled using Dr.View/LINUX software. The ratio of the regional to cerebellar SUV (SUVR) at 40–60 min post-injection was calculated, and averaged SUVR values in the frontal, temporal, parietal and posterior cingulate cortices were considered representative of BF-227 retention in the neocortex (neocortical SUVR).

3.2. Statistical analysis

Statistical comparison of PET and MRI measurements in the four groups was performed via an analysis of variance followed by a Bonferroni multiple comparisons test with a significance level of $p < 0.05$. Statistical comparisons of age and MMSE scores in the four groups were performed using a Kruskal–Wallis test followed by a Dunn's multiple comparison test with a significance level of $p < 0.05$. Correlations between the MMSE score and BF-227 retention in the neocortex or the cerebral atrophy index were examined using a non-parametric Spearman's rank correlation analysis. Correlations between the brain atrophy index and BF-227 retention were determined using Pearson's correlations. A linear model was applied to the data to obtain a correlation coefficient and p value. These analyses were performed using GraphPad Prism5 software (GraphPad, San Diego, CA).

4. Results

In order to confirm the selective binding ability of BF-227 to Aβ deposits, neuropathological examination was initially performed using BF-227 staining of AD temporal brain sections. Senile plaques were selectively stained with BF-227 and the staining pattern coincided well with Aβ immunostaining in an adjacent section (Fig. 1). Strikingly, cored plaques were intensely stained with BF-227, indicating preferential BF-227 binding to dense Aβ fibrils. Next,
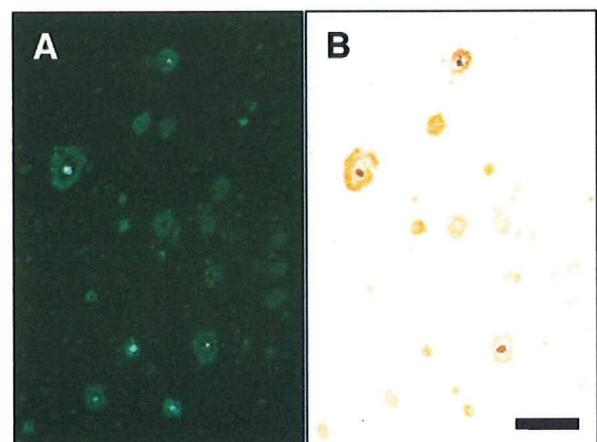

Fig. 1. (A) Neuropathological staining of human brain sections by BF-227. Amyloid plaques are clearly stained with BF-227 in AD temporal brain sections (B) BF-227 staining correlates well with Aβ immunostaining in adjacent sections. Scale bar = 100 μm.
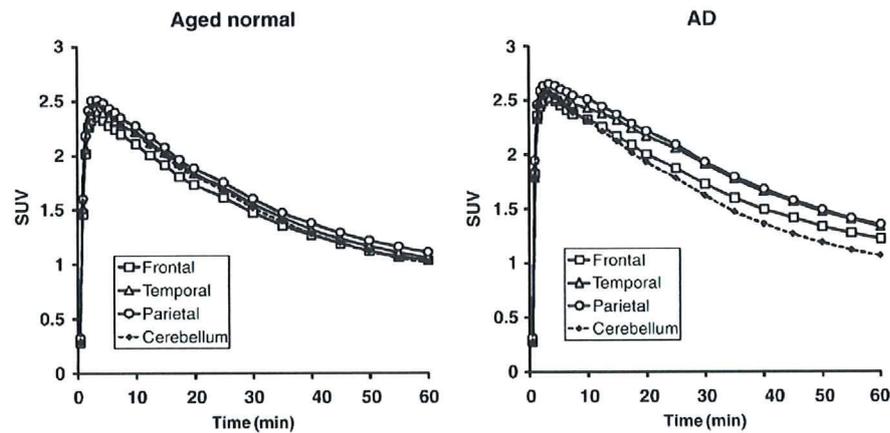
Aged normal   **AD**

Fig. 2. Tissue time activity data for [^{11}C]BF-227–PET. SUV time activity curves of [^{11}C]BF-227 in the frontal cortex, lateral temporal cortex, parietal cortex and cerebellum are shown. Each point represents the mean of 12 control subjects (left) and 15 AD patients (right).

we performed clinical PET using [^{11}C]BF-227 in AD patients, MCI subjects and control subjects. The tissue time activity curves from [^{11}C]BF-227–PET in 15 AD patients and 12 normal controls are shown in Fig. 2. In AD patients, the frontal, temporal and parietal cortices retained [^{11}C]BF-227 to a greater extent at later time points, compared with controls. AD patients showed significantly higher SUVs in the temporal cortex and average neocortex than controls, but not in the cerebellum (Table 2). Therefore, neocortical SUV elevation in AD patients presumably reflects the specific binding of BF-227 to amyloid plaques. Representative images of [^{11}C]BF-227–PET and T1-weighted MRI in a normal control (70-year-old female, MMSE score 29), a MCI non-converter (76-year-old male, MMSE score 27), a MCI converter (85-year-old male, MMSE score 23), and an AD patient (62-year-old female, MMSE score 20) are shown in Fig. 3. Increased BF-227 retention was evident in both the MCI converter and the AD patient, but not in the control subject or the MCI non-converter. In AD patients, BF-227 SUVRs in the frontal, temporal, parietal and posterior cingulate cortices were significantly higher compared to the control subjects and the MCI non-converters (Table 2). A significant elevation of BF-227 SUVR was additionally observed in the frontal, temporal and parietal cortices of MCI converters compared with the control subjects. Consequently, the average neocortical SUVR was significantly higher in the AD patients and MCI converters than in normal subjects and MCI non-converters (Table 2). When a neocortical BF-227 SUVR of 1.11 (1.5SD above control mean) was used as a cut-off, sensitivity of 100% and a specificity of 91.7% in the discrimination between AD patients and normal subjects were achieved.

The voxel-based comparison of gray matter images using SPM5 demonstrated a significant decline of gray matter concentrations in the left ($-28, 14, -26, x, y, z; Z = 5.26$) and the right ($32, 18, -26, x, y, z; Z = 5.24$) medial temporal cortices of AD patients, compared with control subjects (Fig. 4A). SPM2 analysis using the same samples also showed a reduction of gray matter concentrations in nearly the same region and significance (data not shown). We drew the ROI in the parahippocampal area (Fig. 4B) and performed a comparison between the four groups. Significantly lower gray matter intensity was observed in the AD patients, MCI converters and MCI non-converters than in controls (Table 2, Fig. 5). However, age-related changes may be a confounding factor resulting in lower gray matter intensity in MCI groups, as MCI subjects were older than the normal control group. When a parahippocampal ROI value from SPM5 of 0.537 (2SD below control mean) was used as a cut-off, a sensitivity of 80.0% and a specificity of 100% were achieved in the discrimination between AD patients and normal subjects. No significant inter-group difference was observed in the percent global atrophy in VBM analysis due to substantial differences between individuals.

We focused on the comparison between the MCI converters and the non-converters, because these two populations showed no significant difference in age or MMSE scores. A significant inter-group difference was observed in the frontal and the average neocortical SUVR assayed by BF-227–PET, but not in the percent global atrophy or parahippocampal ROI value obtained by VBM–MRI (Table 2, Fig. 5). However, MCI converters showed a tendency toward lower para-hippocampal ROI value derived from SPM5 than MCI non-converters.

Table 2
Summary of imaging measures.

	Normal	MCI non-converter	MCI converter	AD
BF-227 SUV in cerebellum	1.10 ± 0.19	1.08 ± 0.17	1.16 ± 0.22	1.16 ± 0.16
BF-227 SUV in frontal cortex	1.11 ± 0.19	1.10 ± 0.16	1.36 ± 0.33	1.31 ± 0.22
BF-227 SUV in temporal cortex	1.14 ± 0.19	1.19 ± 0.18	1.39 ± 0.28	1.45 ± 0.24[a]
BF-227 SUV in parietal cortex	1.20 ± 0.21	1.20 ± 0.18	1.38 ± 0.29	1.46 ± 0.23
BF-227 SUV in posterior cingulate cortex	1.22 ± 0.22	1.23 ± 0.22	1.39 ± 0.27	1.47 ± 0.21
Average neocortical BF-227 SUV	1.17 ± 0.20	1.18 ± 0.18	1.38 ± 0.29	1.42 ± 0.22[a]
BF-227 SUVR in frontal cortex	1.01 ± 0.06	1.02 ± 0.07	1.16 ± 0.10[a,b]	1.13 ± 0.08[a,b]
BF-227 SUVR in temporal cortex	1.04 ± 0.04	1.10 ± 0.07	1.20 ± 0.07[a]	1.24 ± 0.08[a,b]
BF-227 SUVR in parietal cortex	1.09 ± 0.04	1.12 ± 0.05	1.18 ± 0.07[a]	1.25 ± 0.08[a,b]
BF-227 SUVR in posterior cingulate cortex	1.11 ± 0.06	1.14 ± 0.07	1.20 ± 0.09	1.26 ± 0.05[a,b]
Average neocortical BF-227 SUVR	1.06 ± 0.04	1.09 ± 0.06	1.19 ± 0.07[a,b]	1.22 ± 0.06[a,b]
Percent global atrophy in VBM–MRI	4.24 ± 3.49	7.35 ± 5.94	5.96 ± 3.06	8.53 ± 4.44
Parahippocampal ROI value in VBM–MRI (SPM2)	0.642 ± 0.034	0.569 ± 0.039[a]	0.553 ± 0.044[a]	0.541 ± 0.055[a]
Parahippocampal ROI value in VBM–MRI (SPM5)	0.605 ± 0.034	0.510 ± 0.051[a]	0.473 ± 0.060[a]	0.475 ± 0.068[a]

[a] $p < 0.05$ vs. aged normal.
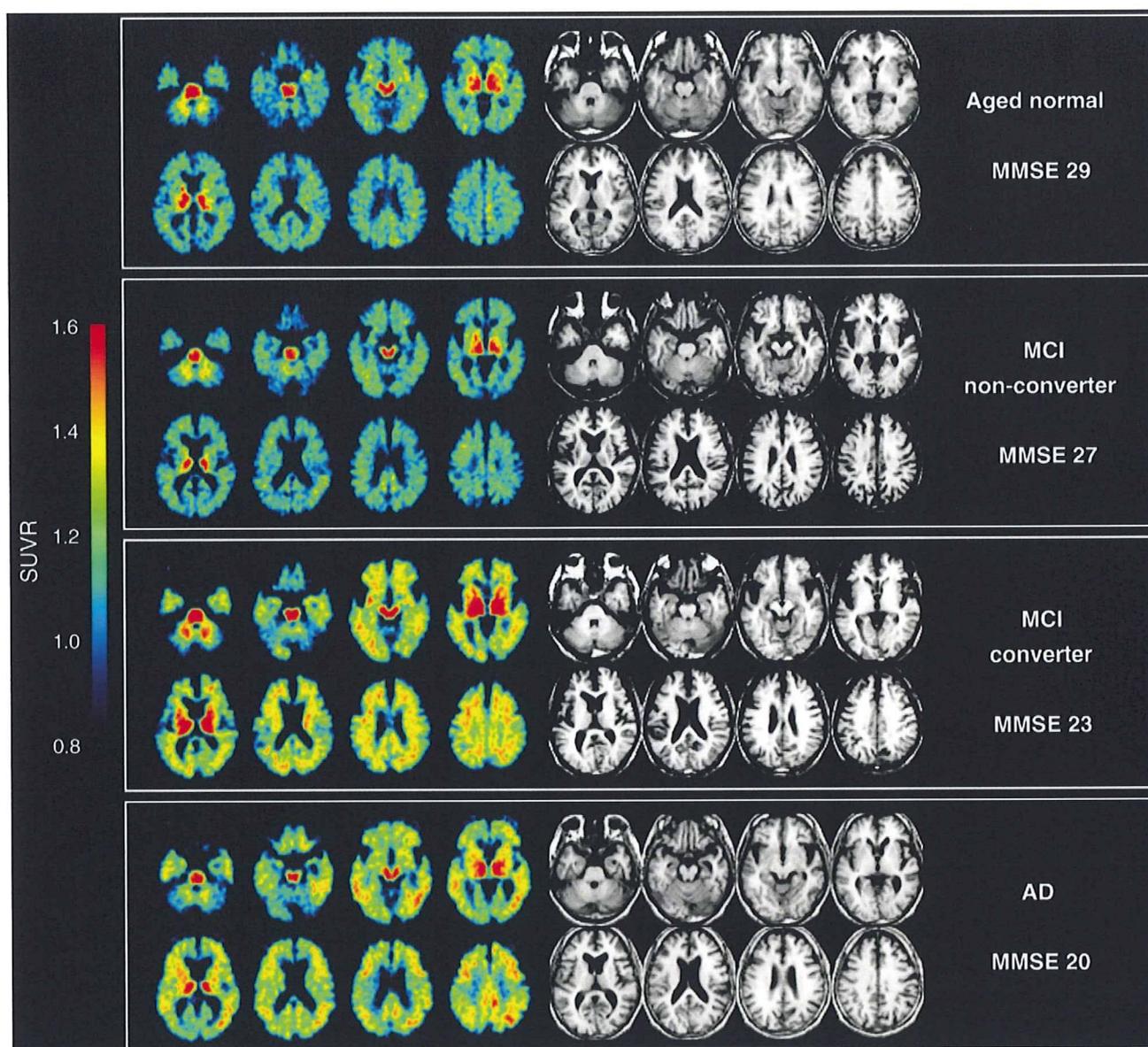[b] $p < 0.05$ vs. MCI non-converter.

Fig. 3. Representative images of [¹¹C]BF-227–PET SUVR between 20 and 40 min post-injection (left) and T1-weighted MRI (right) in a control subject, a MCI non-converter, a MCI converter and an AD subject. The degree of [¹¹C]BF-227 retention is shown by color intensity from yellow to red in the cortex.

When we used a neocortical BF-227 SUVR of 1.11 as a cut-off, we achieved a sensitivity of 100% and a specificity of 71.4% in the discrimination between MCI converters and the MCI non-converters. These values were superior to the results of the parahippocampal ROI value derived from SPM5 (cut-off value: 0.537), which showed a sensitivity of 83.3% and a specificity of 42.9%. These data suggest that BF-227–PET is a better predictor of conversion from MCI to AD than VBM–MRI.

Next, we examined the correlations between MMSE scores and the three volume measurements (Fig. 6). When all subjects ($N = 40$) were included in this analysis, a significant negative correlation was observed in all three measurements (BF-227 SUVR $r = -0.740$, $p < 0.001$; percent global atrophy $r = -0.491$, $p = 0.001$; parahippocampal ROI from SPM2 $r = 0.674$, $p < 0.001$; and parahippocampal ROI from SPM5 $r = 0.687$, $p < 0.001$). However, when we confined the analysis to the combined group of AD patients and MCI converters, we observed a significant correlation only between the percent global atrophy and the MMSE score (Spearman $r = -0.459$, $p = 0.036$). In

contrast, no significant correlation was observed between the parahippocampal ROI from SPM2 and the MMSE (Spearman $r = 0.192$), between the parahippocampal ROI from SPM5 and the MMSE (Spearman $r = 0.181$) or between the BF-227 SUVR in the neocortex and the MMSE (Spearman $r = -0.200$). Finally, no significant correlation was observed between the BF-227 SUVR and the percent global atrophy or parahippocampal atrophy in the analysis of all subjects.

5. Discussion

In the present study, MCI converters were more clearly distinguished from MCI non-converters by BF-227–PET than by VBM–MRI. The MCI non-converters showed a normal distribution of BF-227 except for one case, but also showed lower gray matter density in the parahippocampal gyrus than did normal controls. As a result, BF-227–PET achieved higher sensitivity and specificity in the discrimination between MCI converters and MCI non-converters than did VBM–MRI.
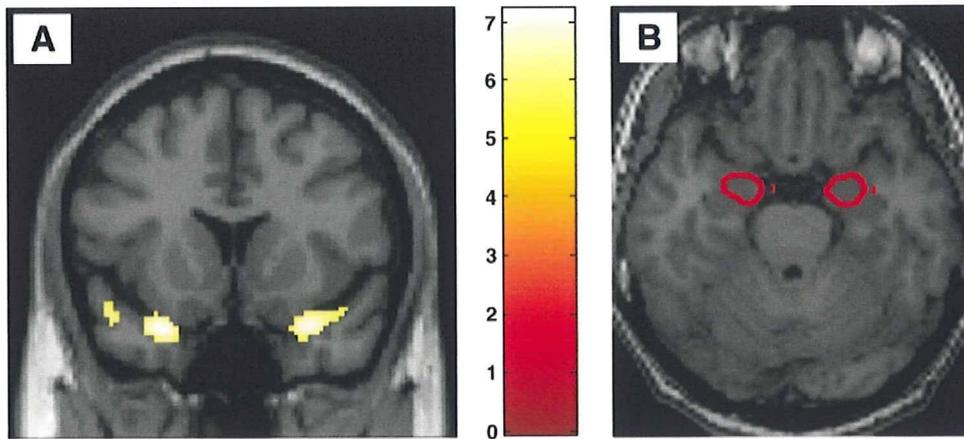
Fig. 4. (A) Areas of reduction in gray matter density of AD patients compared with aged normal controls. $p<0.05$, corrected for multiple comparisons. Left in the image is left in the brain. Color bars represent T values. (B) Regions of interest within the parahippocampal gyrus.

Our results strongly suggest that amyloid imaging using BF-227–PET will be a useful tool to predict conversion from MCI to AD, as previously shown for PIB–PET. [17,18] However, cerebral gray matter loss as determined by VBM–MRI was better correlated with the clinical severity of AD than BF-227–PET. Used together, BF-227–PET and VBM–MRI could be an effective method for the early diagnosis and severity tracking of AD. Our findings may be compatible with the theory that amyloid deposition reaches equilibrium or plateaus at an early stage of AD, making in vivo amyloid imaging useful in the

examination of pre-symptomatic subjects [15,16]. Aβ deposition is a pathological hallmark of AD, but may also occur in normal elderly individuals who do not exhibit apparent cognitive decline. In fact, a PIB–PET study showed that 22% of healthy elderly individuals showed increased cortical PIB binding, indicating the presence of Aβ plaques in these non-symptomatic subjects [15]. A strong relationship between the impairment of episodic memory and PIB binding has also been shown both in subjects with MCI and in the normal population, suggesting that individuals with increased cortical PIB
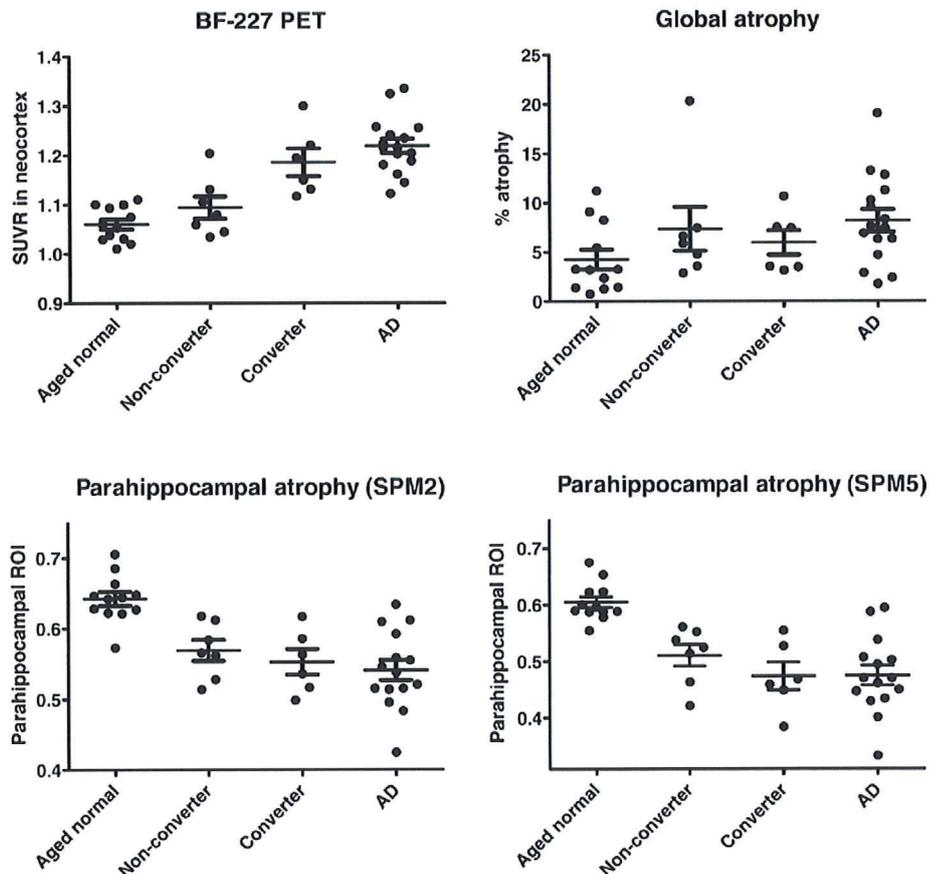

Fig. 5. Comparison of BF-227 SUVR in the neocortex (upper left), the percent global atrophy (upper right), the parahippocampal region of interest (ROI) value from gray matter images processed by SPM2 (lower left) and the parahippocampal ROI value from gray matter images processed by SPM5 (lower right) in control subjects, MCI non-converters, converters and AD patients.
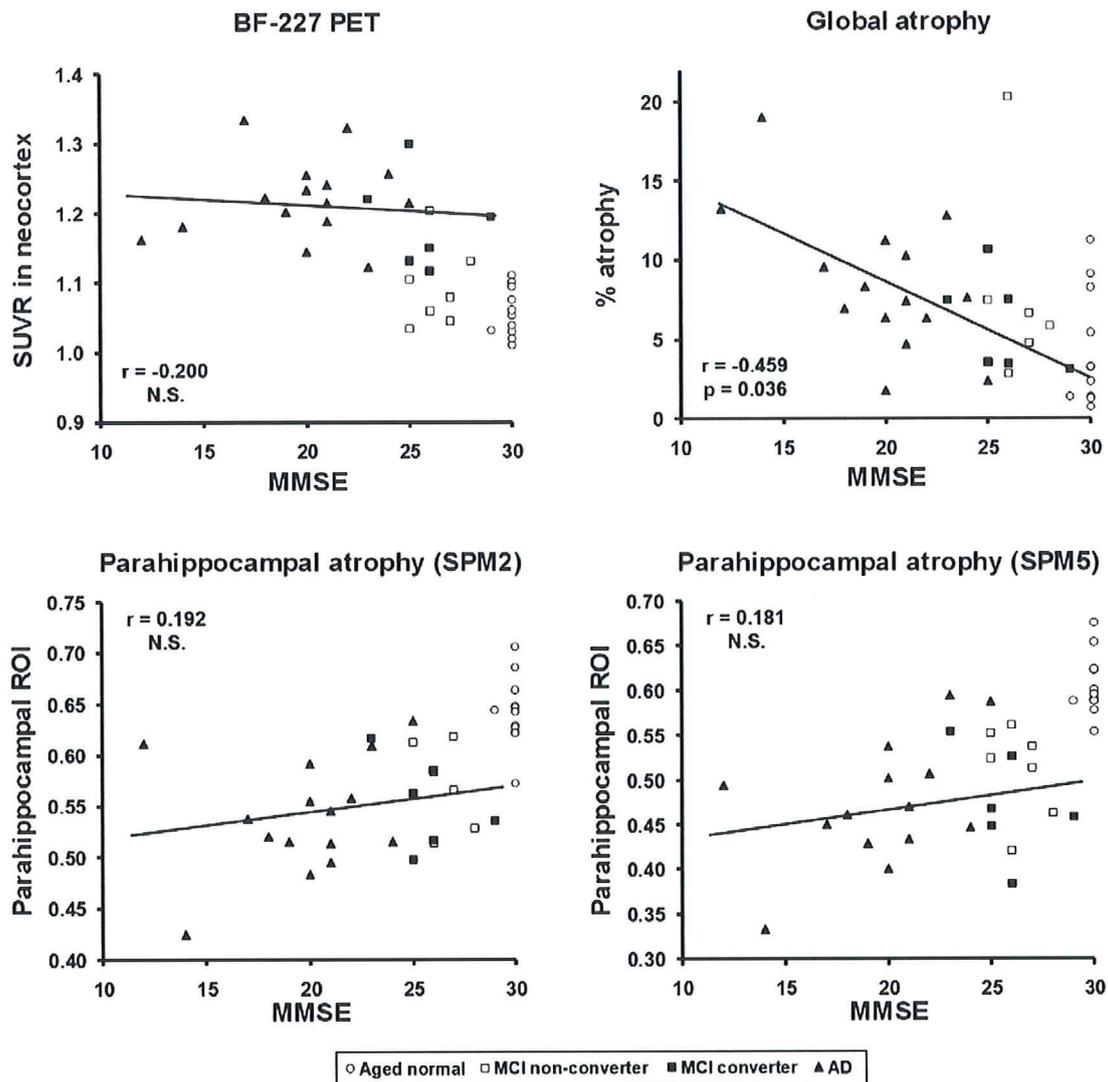
Fig. 6. The correlations of MMSE scores with the BF-227 SUVR in the neocortex (upper left), the percent global atrophy (upper right), the parahippocampal region of interest (ROI) value from gray matter images processed by SPM2 (lower left), and the parahippocampal ROI value from gray matter images processed by SPM5 (lower right). Open circle: control; open square: MCI non-converter; filled square: MCI converter; filled triangle: AD.

binding are proceeding to AD [43]. In our study, almost all normal subjects exhibited a normal distribution of BF-227 in the brain. This finding may suggest a lower sensitivity of diffuse amyloid plaque detection by BF-227 [22]. However, the proportion of amyloid PET-positive individuals in the normal population varies greatly depending on the characteristics of the sample population. Indeed, the mean age of the control subjects in our study was somewhat younger than in previous PIB–PET studies. Therefore, a direct comparison of BF-227–PET with PIB–PET in the same normal population is necessary to compare the ability of these agents to detect early AD pathology. A longitudinal follow-up of amyloid PET-positive cases in the healthy, normal population will also elucidate whether tracer uptake reflects pre-symptomatic detection of AD or a false-positive finding. A follow-up study of the patients with AD using PIB–PET showed that the amyloid deposition remains high but stable, despite decreases in regional glucose metabolism and cognitive function.[44] Our cross-sectional analysis also revealed a plateau of cortical BF-227 uptake in early AD patients, suggesting that amyloid formation reaches a plateau early in the course of AD. A potential limitation of this study is that it used a semiquantitative SUV measure to estimate BF-227 binding to amyloid plaques. The levels of neocortical BF-227 SUV

might be underestimated due to hypoperfusion in AD patients. Quantitative analysis should be performed in future analyses to eliminate the influence of blood flow change.

A previous PIB–PET study found a positive correlation between the rate of whole brain atrophy and amyloid plaque load. [45] However, a recent PET study discovered a discrepancy between regional PIB retention and gray matter loss [38]. Additionally, histopathological analysis revealed no association between Aβ burden and brain atrophy [46]. The present study also found no significant correlation between neocortical BF-227 uptake and global gray matter loss in AD patients, in agreement with these findings. In our correlation analysis of the four measurements with the MMSE scores, we confined our analysis to AD patients and MCI converters because these patients share the same pathological process underlying AD. Therefore, this is more appropriate for the correlation analysis between cognitive function and the degree of Aβ burden or cerebral atrophy induced by the pathological process of AD than an analysis using all samples, including the normal population. In this analysis, the global gray matter loss measured by VBM–MRI was better correlated with MMSE scores than was the Aβ burden measured by BF-227–PET. A similar correlation analysis performed using PIB–PET demonstrated that the

magnitudes of the correlations were greater for hippocampal atrophy than for neocortical PIB retention [38]. The current result, showing no significant correlation of the parahippocampal gray matter density with the MMSE score, seems to be inconsistent with previous PIB–PET data. We believe this discrepancy to be due mainly to differences in the sample population. The analysis in the previous PIB–PET study was performed using all the subjects, including the normal controls; our analysis was confined to AD patients and MCI converters who had already developed severe memory decline and probably substantial neuron loss in the hippocampus. These results suggest that global, rather than parahippocampal, gray matter loss is a potent indicator of dementia severity after the onset of memory loss in AD. We hope to explore the relationship between these imaging measurements and the impairment of episodic memory function in a future study.

It has been reported that the degree or rate of change of cerebral atrophy as measured by MRI analysis is closely related to the clinical progression of dementia [29,30]. Karas et al. performed a VBM–MRI analysis to examine the global and regional gray matter loss in normal, MCI and AD subjects, finding a significantly lower global gray matter volume in the AD subjects and an intermediate volume in the MCI subjects [31]. They followed the MCI subjects and observed greater gray matter loss in the MCI converters than in non-converters [37]. Another study also revealed different patterns of gray matter density distribution between MCI converters and non-converters [35]. From these findings, it appears that gray matter loss in VBM is a good indicator of conversion from MCI to AD. We failed to demonstrate significant inter-group differences between the MCI converters and non-converters, although the MCI converters showed a tendency toward lower parahippocampal gray matter density than did the non-converters. This, however, may be due to the small sample size and insufficient follow-up period (over two years) of the MCI subjects in this study. For example, one MCI non-converter in our study showed an abnormality in both the BF-227 SUVR and parahippocampal gray matter density; extending the follow-up period of the MCI subjects would likely result in more consistent correlation between MCI conversion to AD and the described measurements. Additional longitudinal studies are also needed to confirm the findings we have obtained and to examine the time course of AD, including changes in the pre-symptomatic subjects, and to determine the relationship between amyloid deposition and brain atrophy as underlying factors in the pathogenesis of AD.

Acknowledgements

References

[1] Blennow K, de Leon MJ, Zetterberg H. Alzheimer's disease. Lancet 2006;368: 387–403.
[2] Drachman DA. Aging of the brain, entropy, and Alzheimer disease. Neurology 2006;67:1340–52.
[3] Braak H, Braak E. Neuropathological stageing of Alzheimer-related changes. Acta Neuropathol 1991;82:239–59.
[4] Arnold SE, Hyman BT, Flory J, Damasio AR, Van Hoesen GW. The topographical and neuroanatomical distribution of neurofibrillary tangles and neuritic plaques in the cerebral cortex of patients with Alzheimer's disease. Cereb Cortex 1991;1:103–16.
[5] Mouton PR, Martin LJ, Calhoun ME, Dal Forno G, Price DL. Cognitive decline strongly correlates with cortical atrophy in Alzheimer's dementia. Neurobiol Aging 1998;19:371–7.
[6] Masters CL, Cappai R, Barnham KJ, Villemagne VL. Molecular mechanisms for Alzheimer's disease: implications for neuroimaging and therapeutics. J Neurochem 2006;97:1700–25.
[7] Nordberg A. PET imaging of amyloid in Alzheimer's disease. Lancet Neurol 2004;3: 519–27.
[8] Villemagne VL, Rowe CC, Macfarlane S, Novakovic KE, Masters CL. Imaginem oblivionis: the prospects of neuroimaging for early detection of Alzheimer's disease. J Clin Neurosci 2005;12:221–30.
[9] Mathis CA, Klunk WE, Price JC, DeKosky ST. Imaging technology for neurodegenerative diseases: progress toward detection of specific pathologies. Arch Neurol 2005;62:196–200.
[10] Nordberg A. Amyloid imaging in Alzheimer's disease. Curr Opin Neurol 2007;20: 398–402.
[11] Small GW, Kepe V, Ercoli LM, Siddarth P, Bookheimer SY, Miller KJ, et al. PET of brain amyloid and tau in mild cognitive impairment. N Engl J Med 2006;355:2652–63.
[12] Klunk WE, Engler H, Nordberg A, Wang Y, Blomqvist G, Holt DP, et al. Imaging brain amyloid in Alzheimer's disease with Pittsburgh Compound-B. Ann Neurol 2004;55:306–19.
[13] Price JC, Klunk WE, Lopresti BJ, Lu X, Hoge JA, Ziolko SK, et al. Kinetic modeling of amyloid binding in humans using PET imaging and Pittsburgh Compound-B. J Cereb Blood Flow Metab 2005;25:1528–47.
[14] Lopresti BJ, Klunk WE, Mathis CA, Hoge JA, Ziolko SK, Lu X, et al. Simplified quantification of Pittsburgh Compound B amyloid imaging PET studies: a comparative analysis. J Nucl Med 2005;46:1959–72.
[15] Rowe CC, Ng S, Ackermann U, Gong SJ, Pike K, Savage G, et al. Imaging beta-amyloid burden in aging and dementia. Neurology 2007;68:1718–25.
[16] Mintun MA, Larossa GN, Sheline YI, Dence CS, Lee SY, Mach RH, et al. [^{11}C]PIB in a nondemented population: potential antecedent marker of Alzheimer disease. Neurology 2006;67:446–52.
[17] Fripp J, Bourgeat P, Acosta O, Raniga P, Modat M, Pike KE, et al. Appearance modeling of ^{11}C PiB PET images: characterizing amyloid deposition in Alzheimer's disease, mild cognitive impairment and healthy aging. Neuroimage 2008;43:430–9.
[18] Forsberg A, Engler H, Almkvist O, Blomquist G, Hagman G, Wall A, et al. PET imaging of amyloid deposition in patients with mild cognitive impairment. Neurobiol Aging 2008;29:1456–65.
[19] Okamura N, Suemoto T, Shimadzu H, Suzuki M, Shiomitsu T, Akatsu H, et al. Styrylbenzoxazole derivatives for in vivo imaging of amyloid plaques in the brain. J Neurosci, 2004;24:2535–41.
[20] Okamura N, Furumoto S, Funaki Y, Suemoto T, Kato M, Ishikawa Y, et al. Binding and safety profile of novel benzoxazole derivative for in vivo imaging of amyloid deposits in Alzheimer's disease. Geriatr Gerontol Int 2007;7:393–400.
[21] Furumoto S, Okamura N, Iwata R, Yanai K, Arai H, Kudo Y. Recent advances in the development of amyloid imaging agents. Curr Top Med Chem 2007;7:1773–89.
[22] Kudo Y, Okamura N, Furumoto S, Tashiro M, Furukawa K, Maruyama M, et al. 2-(2-[2-Dimethylaminothiazol-5-yl]Ethenyl)-6-(2-[Fluoro]Ethoxy)Benzoxazole: A novel PET agent for in vivo detection of dense amyloid plaques in Alzheimer's disease patients. J Nucl Med 2007;48:553–61.
[23] Fodero-Tavoletti MT, Mulligan RS, Okamura N, Furumoto S, Rowe CC, Kudo Y, et al. In vitro characterization of BF227 binding to α-synuclein/Lewy Bodies. Eur J Pharmacol 2009;617:54–8.
[24] Ishii K, Hashimoto M, Kimura Y, Sakata M, Oda K, Kawasaki K, et al. Direct comparison of in vivo accumulation of ^{11}C-PIB and ^{11}C-BF227 in Alzheimer's disease. Alzheimer's and Dementia, vol. 4, Issue 4; July 2008. p. T49. Supplement 1.
[25] Tiraboschi P, Hansen LA, Thal LJ, Corey-Bloom J. The importance of neuritic plaques and tangles to the development and evolution of AD. Neurology 2004;62:1984–9.
[26] Price JL, Morris JC. Tangles and plaques in nondemented aging and "preclinical" Alzheimer's disease. Ann Neurol 1999;45:358–68.
[27] Morris JC, Storandt M, Miller JP, McKeel DW, Price JL, Rubin EH, et al. Mild cognitive impairment represents early-stage Alzheimer disease. Arch Neurol 2001;58:397–405.
[28] Wang J, Dickson DW, Trojanowski JQ, Lee VM. The levels of soluble versus insoluble brain Abeta distinguish Alzheimer's disease from normal and pathologic aging. Exp Neurol 1999;158:328–37.
[29] Fox NC, Crum WR, Scahill RI, Stevens JM, Janssen JC, Rossor MN. Imaging of onset and progression of Alzheimer's disease with voxel-compression mapping of serial magnetic resonance images. Lancet 2001;358:201–5.
[30] Jack Jr CR, Shiung MM, Gunter JL, O'Brien PC, Weigand SD, Knopman DS, et al. Comparison of different MRI brain atrophy rate measures with clinical disease progression in AD. Neurology 2004;62:591–600.
[31] Karas GB, Scheltens P, Rombouts SA, Visser PJ, van Schijndel RA, Fox NC, et al. Global and local gray matter loss in mild cognitive impairment and Alzheimer's disease. Neuroimage 2004;23:708–16.
[32] Killiany RJ, Gomez-Isla T, Moss M, Kikinis R, Sandor T, Jolesz F, et al. Use of structural magnetic resonance imaging to predict who will get Alzheimer's disease. Ann Neurol 2000;47:430–9.
[33] Bell-McGinty S, Lopez OL, Meltzer CC, Scanlon JM, Whyte EM, Dekosky ST, et al. Differential cortical atrophy in subgroups of mild cognitive impairment. Arch Neurol 2005;62:1393–7.
[34] Chetelat G, Landeau B, Eustache F, Mezenge F, Viader F, de la Sayette V, et al. Using voxel-based morphometry to map the structural changes associated with rapid conversion in MCI: a longitudinal MRI study. Neuroimage 2005;27:934–46.
[35] Bozzali M, Filippi M, Magnani G, Cercignani M, Franceschi M, Schiatti E, et al. The contribution of voxel-based morphometry in staging patients with mild cognitive impairment. Neurology 2006;67:453–60.